arXiv:1607.00923v1 [math.AP] 4 Jul 2016

A viscous layer model for a shallow water free surface flow

July 5, 2016

François James*, Pierre-Yves Lagrée^o and Mathilde Legrand*
^{o} Sorbonne Universités, UPMC Univ Paris 06, CNRS, UMR 7190,
Institut Jean Le Rond d'Alembert, F-75005 Paris, France
* Mathématiques – Analyse, Probabilités, Modélisation – Orléans (MAPMO),
Université d'Orléans & CNRS UMR 7349, BP 6759, F-45067 Orléans Cedex 2, France
francois.james@univ-orleans.fr

Abstract

Shallow Water equations are widely used at several scales for liquid flows when the depth is smaller than the longitudinal scale. They are based on assumptions on the velocity profile which allow to estimate its shape factor and the shear stress at the wall to close the system of equations. We present here a two layers decompositon between an ideal fluid and a viscous layer, in the spirit of IBL (Interactive Boundary Layer) or IVI (Inviscid Viscous Interaction) introduced in aeronautics. It means that the two layers interact. The displacement thickness of the viscous layer and the order of magnitude of the shear stress at the wall are supposed small and of same order of magnitude. We use this small parameter for expansion and obtain a coupled system of two interacting layers, the viscous layer being then a kind of apparent topography due to the displacement thickness. We show the link with classical Shallow Water equations. The assumption on the velocity profile shape is rejected in the viscous layer, which makes assumptions on profiles (shape factor and wall shear stress) more precise. We test the final system on some classical cases like the starting flow, the flow over bump at several Froude regimes. We finally focus on the flow over a bump in subcritical flows. The computed wall shear stress in this configuration presents some characteristic features of the influence of the boundary layer, it depends on the topography, and moreover its maximum is reached before the top of the bump, which is impossible in classical Shallow Water equations. Also, an additional term with the same magnitude as the shear stress appears in the system, which can be interpreted as a correction to the pressure.

Keywords: viscous layer, von Kármán equation, boundary layer, Prandtl equation, shallow water, friction
2010 AMS subject classifications: Primary: 35B40, 35D30, 35L60, 35Q92, 49K20

Introduction

Many phenomena in maritime or fluvial hydraulics involve free surface flows in shallow waters. The so-called shallow water equations were introduced by Saint-Venant in 1871 [4] for studying floods and tides. Since then, the model has been widely extended and is used in the modelling and numerical simulation of a number of natural or manmade phenomena such as river flow [17, 7], flood forecasting [8], pollutant transport [28, 18], dam-break [1, 33], tsunami [16, 21, 26], overland flow [13, 32, 11], soil erosion [25].

The shallow water system can be obtained from the incompressible Navier-Stokes equations under several hypotheses, the main one being that the characteristic wavelength is much larger than the water depth. Two consequences follow then: the hydrostatic pressure law, and the viscosity vanishing in the horizontal direction. Next, to proceed from Navier-Stokes to shallow water, we integrate the equations along the vertical direction. At this point, we have to be careful about the vertical velocity profile, which on the one hand has to be

approximated to deal with nonlinearities, but on the other hand drives the bottom boundary condition, hence the friction phenomena.

Two classical assumptions on the velocity profile lead to explicit integrations. First, a viscous Poiseuille-like (i.e. parabolic) profile on the whole water depth gives rise to a linear (with respect to the mean velocity) friction term, sometimes referred to as laminar friction. Even simpler, the constant vertical profile, somehow corresponding to an ideal fluid, has the main drawback that by construction the boundary condition at bottom disappears (non penetration for an ideal fluid). Hence there is no friction term in the integrated equations. This corresponds to the original model proposed by Saint-Venant, which he obtained by completely different means. Friction has to be added afterwards, using empirical laws (Manning, Chézy,...)[9]. The main drawback of these two points of view is the non-adaptability of the viscous term due to large velocity variations, so that the assumed profiles (parabolic or flat) do not hold. We propose here a more flexible coupled system based on a supplementary viscous layer study.

More precisely the aim of this paper is to understand how the viscous no-slip boundary condition gives rise to the friction term in the integrated system. This is done by assuming the existence of a viscous layer above the ground, with thickness quantified by a parameter $\overline{\delta} > 0$, which is related to the inverse of the Reynolds number of the fluid. Here $\overline{\delta}$ will be small but not necessarily vanishing as in classical boundary layer analysis. Above this layer lies an ideal fluid. Integrating the incompressibility equation under this assumption leads to the same conservation equation on the fluid depth. On the contrary, the integration of the momentum equation exhibits major differences. Indeed, it turns out that the order of magnitude of the friction term, which results from the parietal constraints, is precisely $\overline{\delta}$, while the above mentioned Poiseuille profile leads to a $\overline{\delta}^2$ order of magnitude (see part 1.3). Motivated by this precise quantification of the intensity of friction, we introduce a new closure for the flux momentum. It can be interpreted as an additional pressure law, with the same magnitude $\overline{\delta}$, so that both terms vanish for an ideal fluid, that is $\overline{\delta} = 0$.

At this stage, we obtain a system of two equations which are similar in structure with the usual shallow water system, but involving several additional unknowns functions precisely related to the viscous layer. Following classical methodology in aerodynamics, see e.g. [29], the second step consists therefore in a careful analysis of this layer, through the Prandtl equation, which is integrated along the vertical axis to obtain the so-called von Kármán equation. It drives the evolution of the so-called displacement thickness δ_1 (see Figure 1), which is involved in the definition of the corrective pressure mentioned above, and can be interpreted as some physical thickness of the viscous layer. The system has to be complemented by the velocity equation of the ideal fluid, since it is involved in the von Kármán equation. Together with some assumptions on the vertical velocity profile in the viscous layer, this leads to a system of four equations. In practice we will discuss the effects for flows over short bumps. The acceleration induced by the bump will change a lot the basic flow so that the shape velocity profile is no longer a half Poiseuille nor a flat one. This study aims to understand this kind of flows which are not taken into account by the shallow water equations themselves. The major limit of the following theory is the necessity of the ideal fluid/viscous layer decomposition.

The outline of the paper is as follows. In a first section we recall the Navier-Stokes system, and state the long wave approximation which is convenient for shallow water approximation. Next we turn to the viscous layer analysis, and derive Prandtl and von Kármán equations. Vertical velocity profiles are also introduced. The third section is devoted to the derivation of the Extended shallow water system leading to our new model (3.8)-(3.10). In Section 4 we derive some formal properties of the model, together with analytical steady state solutions. Finally, we evidence several properties of the model by numerical simulations, the purpose of the paper not being to develop sharp discretizations.

1 From Navier-Stokes to shallow waters

In this section we recall how classical models for shallow waters are obtained from Navier-Stokes equations. The first assumption is a long wave approximation, stating that indeed we deal with a thin layer of water. Next, we integrate along the vertical direction, assuming a given velocity profile on the whole water depth.

1.1 Navier-Stokes equations

We consider a fluid in a time-dependant domain $\Omega_t = \mathbb{R} \times \{f_b(x) \leq y \leq \eta(t,x)\}$ (see figure 1), where the first dimension x is horizontal and with infinite extension, the second one y is vertical. The fluid is limited by the ground, represented by a function $y = f_b(x)$, and some free surface $y = \eta(t,x)$. The ground is a given function

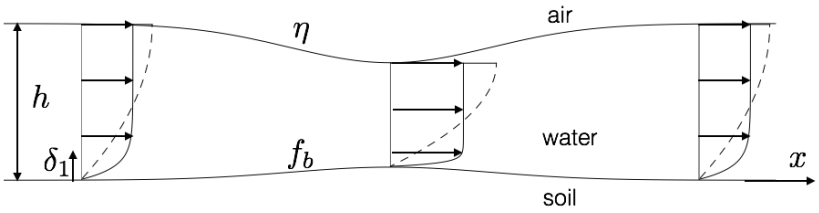

Figure 1: Domain under consideration: the water layer is defined by the depth h, the bottom is a given function f_b and η is the free surface. Two families of velocity profiles for the flow over the topography, first with the usual half-Poiseuille description (dashed) (see 1.3 for the explanations), and second with the flat profile with a boundary layer (plain). Note the shear (slope of the velocity at the wall) is completely different in both descriptions.

(no erosion or ground modification), whereas the free surface is an unknown of the problem. The water height is $h = \eta - f_b$. In this study, the properties of the air above the free surface are completely neglected.

Our starting point to describe the liquid layer is the dimensionless Navier-Stokes equations for an incompressible Newtonian fluid in laminar flow [29]:

$$\partial_x u + \partial_y v = 0 \tag{1.1}$$

$$\partial_t u + u\partial_x u + v\partial_y u = -\partial_x p + \frac{1}{Re_h}\Delta u \tag{1.2}$$

$$\partial_t v + u\partial_x v + v\partial_y v = -\partial_y p - \frac{1}{Fr^2} + \frac{1}{Re_h}\Delta v \tag{1.3}$$

where

- $\mathbf{U} = (u, v)$ is the velocity vector
- $Re_h = \frac{u_0 h_0}{\nu}$ is the Reynolds number expressing the ratio between the inertia force and the viscosity
- $Fr = \frac{u_0}{\sqrt{g h_0}}$ is the Froude number, ratio between the kinetic and potential energies
- p is the pressure

Remark 1.1. *Nondimensionalization has been made with the same characteristic length for the abscissa and the ordinate, and corresponds for instance to the mean water depth h_0, that appears in the Reynolds and Froude numbers.*

Remark 1.2. *We consider in this work only laminar flows because the asymptotics from the Navier-Stokes equations is clearer, and moreover the resulting description is quantitative. A similar study can be made with a modified Reynolds tensor and we can hope it leads at least to some qualitative description.*

The system is complemented with the following boundary conditions:

- bottom: no-slip $u = v = 0$ for $y = f_b(x)$
- free surface $y = \eta(t, x)$
  - kinematic boundary condition: $v = \partial_t \eta + u\partial_x \eta$
  - continuity of the stress tensor: $\sigma \cdot \mathbf{n} = \mathbf{0}$, where $\sigma = \begin{pmatrix} 2\partial_x u - p & \partial_x v + \partial_y u \\ \partial_y u + \partial_x v & 2\partial_y v - p \end{pmatrix}$ is the stress tensor and $n = \begin{pmatrix} \partial_x \eta \\ -1 \end{pmatrix}$ is the normal to the free surface.

1.2 Long wave scaling

Up to now, no hypothesis has been taken into account for the size order of the characteristic quantities u_0, h_0. We have in mind applications to rivers or coastal flows where the following conditions may be observed:

- the horizontal velocity has small variation along the vertical;
- the Reynolds number is large;
- the vertical velocity is small compared to the horizontal velocity.

Let us start by investigating the third one, which justifies the following scaling for the velocities:

$$v = \varepsilon \tilde{v} \qquad u = \tilde{u}.$$

Then the mass conservation equation (1.1) enforces also a scaling for the space variables $y \ll x$ since

$$0 = \partial_x u + \partial_y v = \partial_x \tilde{u} + \varepsilon \partial_y \tilde{v}.$$

Hence there are two options for the variable scaling:

1. Long wave hypothesis. We introduce the aspect ratio of the system $\varepsilon = \frac{h_0}{L}$. The scaling is

   $$x = \frac{\tilde{x}}{\varepsilon} \qquad y = \tilde{y}.$$

   This scaling is the same as a nondimensionalization of the Navier-Stokes equations with a characteristic length L for the domain and a characteristic physical height h_0. This scaling has to be complemented with $t = \frac{\tilde{t}}{\varepsilon}$. So, the long wave hypothesis needs a long time study. Furthermore, since $f_b(x) = \tilde{f}_b(\tilde{x})$, we have $f_b'(x) = \varepsilon \tilde{f}_b{}'(\tilde{x})$ and so the physical slope needs to be small enough.

2. Thin layer scaling:

   $$x = \tilde{x} \qquad y = \varepsilon \tilde{y} \qquad t = \tilde{t}$$

   This scaling restricts the study of small vertical velocity only to a thin water depth which tends to zero when $\varepsilon \to 0$. It is the classical scaling used in the boundary layer approach.

So, the only scaling which is compatible with a small vertical velocity compared to the horizontal velocity is the long wave scaling. Let us see the consequences for the set of equations (1.1)-(1.3) and the boundary conditions.

$$\begin{aligned}
\partial_{\tilde{x}} \tilde{u} + \partial_{\tilde{y}} \tilde{v} =& 0 \\
\varepsilon \left[\partial_{\tilde{t}} \tilde{u} + \tilde{u}\partial_{\tilde{x}} \tilde{u} + \tilde{v}\partial_{\tilde{y}} \tilde{u}\right] =& -\varepsilon \partial_{\tilde{x}} \tilde{p} + \frac{1}{Re_h}\left[\varepsilon^2 \partial_{\tilde{x}}^2 \tilde{u} + \partial_{\tilde{y}}^2 \tilde{u}\right] \qquad (1.4) \\
\varepsilon^2 \left[\partial_{\tilde{t}} \tilde{v} + \tilde{u}\partial_{\tilde{x}} \tilde{v} + \tilde{v}\partial_{\tilde{y}} \tilde{v}\right] =& -\frac{1}{Fr^2} - \partial_{\tilde{y}} \tilde{p} + \frac{\varepsilon}{Re_h}\left[\varepsilon^2 \partial_{\tilde{x}}^2 \tilde{v} + \partial_{\tilde{y}}^2 \tilde{v}\right] \qquad (1.5) \\
\tilde{u} = \tilde{v} =& 0 \qquad \text{at} \qquad \tilde{y} = \tilde{f}_b \\
\tilde{v} = \partial_{\tilde{t}} \tilde{\eta} + & \tilde{u}\partial_{\tilde{x}} \tilde{\eta} \qquad \text{at} \qquad \tilde{y} = \tilde{\eta} \\
\begin{pmatrix} \varepsilon\big((2\varepsilon\partial_{\tilde{x}} \tilde{u} - \tilde{p})\partial_{\tilde{x}} \tilde{\eta} - \varepsilon\partial_{\tilde{x}} \tilde{v}\big) - \partial_{\tilde{y}} \tilde{u} \\ \varepsilon\big(\partial_{\tilde{x}} \tilde{\eta}(\partial_{\tilde{y}} \tilde{u} + \varepsilon\partial_{\tilde{x}} \tilde{v}) - 2\partial_{\tilde{y}} \tilde{v}\big) - \tilde{p} \end{pmatrix} =& \begin{pmatrix} 0 \\ 0 \end{pmatrix} \qquad \text{at} \qquad \tilde{y} = \tilde{\eta}
\end{aligned}$$

Taking an approximation at order $O(\varepsilon)$ leads to:

- Simplified version of the stress tensor continuity at the free surface: $\tilde{p} = 0$ and $\partial_{\tilde{y}} \tilde{u} = 0$ at $\tilde{y} = \tilde{\eta}$.
- Hydrostatic pressure with (1.5) and $\tilde{p} = 0$ at the surface:

  $$\partial_{\tilde{y}} \tilde{p} = -\frac{1}{Fr^2} \Longleftrightarrow \tilde{p} = \frac{1}{Fr^2}(\tilde{\eta} - \tilde{y}).$$

  This result for pressure at order $O(\varepsilon)$ is already observed, see for instance [20], chapter 5.

- Cancellation of the viscosity in the x direction in (1.4):

  $$\partial_{\tilde{t}} \tilde{u} + \tilde{u}\partial_{\tilde{x}} \tilde{u} + \tilde{v}\partial_{\tilde{y}} \tilde{u} = -\partial_{\tilde{x}} \tilde{p} + \frac{1}{\varepsilon Re_h}\partial_{\tilde{y}}^2 \tilde{u}.$$

Remark 1.3. *We emphasize here that the above properties, which are classical shallow water hypotheses, are brought out solely by the long wave approximation.*

To summarize, the long wave approximation of the Navier-Stokes equations consists of the following set of equations:

$$\partial_{\tilde{x}}\tilde{u} + \partial_{\tilde{y}}\tilde{v} = 0 \tag{1.6}$$

$$\partial_{\tilde{t}}\tilde{u} + \tilde{u}\partial_{\tilde{x}}\tilde{u} + \tilde{v}\partial_{\tilde{y}}\tilde{u} = -\partial_{\tilde{x}}\tilde{p} + \frac{1}{\varepsilon Re_h}\partial^2_{\tilde{y}}\tilde{u} \tag{1.7}$$

$$\partial_{\tilde{y}}\tilde{p} = -\frac{1}{Fr^2} \tag{1.8}$$

$$\tilde{u} = \tilde{v} = 0 \qquad \text{at} \qquad \tilde{y} = \tilde{f}_b \tag{1.9}$$

$$\tilde{v} = \partial_{\tilde{t}}\tilde{\eta} + \tilde{u}\partial_{\tilde{x}}\tilde{\eta} \qquad \text{at} \qquad \tilde{y} = \tilde{\eta} \tag{1.10}$$

$$\tilde{p} = 0, \qquad \partial_{\tilde{y}}\tilde{u} = 0 \qquad \text{at} \qquad \tilde{y} = \tilde{\eta} \tag{1.11}$$

This will be our reference system for the remaining of this article. Hence, from now on we shall drop the tildes when referring to the variables and unknowns of the previous system of equations.

Notice that in this setting the effective Reynolds number is εRe_h, which takes into account the aspect ratio of the system $\varepsilon = h_0/L$. We shall come back more precisely on this when studying the Prandtl equation below, but notice that the actual ideal fluid limit here corresponds to $\varepsilon Re_h \to \infty$, leading to the hydrostatic Euler system:

$$\partial_x u + \partial_y v = 0 \tag{1.12}$$

$$\partial_t u + u\partial_x u + v\partial_y u = -\partial_x p \tag{1.13}$$

$$\partial_y p = -\frac{1}{Fr^2} \tag{1.14}$$

$$\partial_t \eta + u\partial_x \eta = v \qquad \text{at } y = \eta \tag{1.15}$$

As usual, the no-slip boundary condition (1.9) is not relevant for the ideal fluid and has to be replaced by the non-penetration condition

$$-u{f_b}' + v = 0 \qquad \text{at } y = f_b. \tag{1.16}$$

Recovering some connection between the ideal fluid equations and the no-slip condition is precisely the aim of the viscous layer theory, which we will present in Section 2.

Audusse et al. propose in [3] to consider in the long-wave approximation of both Euler and Navier-Stokes system several layers and integrate over each layer. Similarly to finite volume numerical methods, matter and momentum fluxes are taken into account at each interface between the layers. Therefore they are faced with a superposition of shallow water systems each one interacting with its neighbours. This can be interpreted as a discretization in the vertical direction of the two-dimensional systems. Our method is different in that the two layers have different status, based on physical motivations. The relative thickness of each part is not fixed but evolves in time.

1.3 Shallow water equations

The aim of this paragraph is to recall the classical way to obtain shallow water equations by vertical integration over the whole water depth, first in the long-wave approximation of the Euler equations, then in the long-wave approximation of the Navier-Stokes equations.

Averaging the Euler system (1.12)-(1.16) over the water depth leads to the so-called shallow water model without friction. We introduce the natural averaged velocity.

Definition 1.4. *The averaged velocity U is defined by* $hU = \displaystyle\int_{f_b}^{\eta} u\,dy$.

With this construction, U is defined h-a.e. (i.e. only for $h > 0$). Then straightforward computations (see Section 3 below for details) lead to

$$\partial_t h + \partial_x(hU) = 0, \tag{1.17}$$

$$\partial_t(hU) + \partial_x\left(\int_{f_b}^{\eta} u^2\,dy\right) = -\frac{1}{Fr^2}h(\partial_x h + f_b'), \tag{1.18}$$

The momentum equation above requires some closure for the flux. This can be achieved by assuming a flat velocity profile over the water depth, which is compatible with the ideal fluid assumption. This leads to $\int_{f_b}^{\eta} u^2\,dy = \frac{1}{h}(\int_{f_b}^{\eta} u\,dy)^2$, hence the momentum equation becomes

$$\partial_t(hU) + \partial_x\left(hU^2 + \frac{h^2}{2Fr^2}\right) = -\frac{hf_b'}{Fr^2}. \tag{1.19}$$

Equations (1.17) and (1.19) correspond to the equations derived by de Saint-Venant by completely different means, with the additional topography term.

If we proceed in an analogous way from the Navier-Stokes equations in long wave scaling, we obtain a viscous shallow water where the water depth conservation is the same as before (1.17), but the momentum equation becomes

$$\partial_t(hU) + \partial_x\left(\int_{f_b}^{\eta} u^2\,dy\right) = -\frac{1}{Fr^2}h(\partial_x h + f_b') - \frac{1}{\varepsilon Re}\partial_y u|_{y=f_b}. \tag{1.20}$$

Once again, without the presence of complementary equations, a closure is needed for the u-profile over all the water depth. Explicit formulæ are given in [19] depending of the flow index of the fluid. Focusing on a Newtonian fluid with a negative constant slope, the balance between the friction and the driving force of the slope gives a parabolic solution for u, the half-Poiseuille or Nusselt solution: $u(t,x,y) = -\frac{3U_m}{2}(\frac{y-f_b}{h})(\frac{y-f_b}{h} - 2)$ with $U_m = -\frac{\varepsilon Re_h f_b'}{3Fr^2}h^2$ a positive constant. In the general case, even if the invariance is not conserved, a similar form is chosen for the velocity profile but the deviating is expressed with a variable amplitude instead of a constant one: $u(t,x,y) = -\frac{3}{2}U(t,x)\frac{y-f_b}{h}(\frac{y-f_b}{h} - 2)$. Nevertheless, the explicit integration gives the following system:

$$\partial_t h + \partial_x(hU) = 0 \tag{1.21}$$

$$\partial_t(hU) + \partial_x\left(\frac{6}{5}hU^2 + \frac{h^2}{2Fr^2}\right) = -\frac{hf_b'}{Fr^2} - \frac{3}{\varepsilon Re_h}\frac{U}{h}. \tag{1.22}$$

The friction term which naturally appears in this derivation is $-\frac{3}{\varepsilon Re_h}\frac{U}{h}$. It is indeed linear with respect to the mean velocity U, and is usually referred to as the laminar friction term.

An alternative way to reintroduce some viscosity in the inviscid shallow water equations (1.17)-(1.19) is to put a posteriori some friction term similar to the one in the Poiseuille-shallow water (1.22). A general form for such a friction term is $C_\ell\frac{U}{h}$ to be consistent with the previous equation, but a large family of empirical friction laws involves a C_ℓ depending on U as well, for instance Chézy, Manning, see [9] for a bibliographical study.

2 Viscous layer analysis

We turn now to the main step towards the model we look for. It mainly consists in dividing the fluid in two layers

- An ideal fluid layer dealing with the free surface;
- A thin viscous layer with the no-slip condition at the bottom.

Between these layers lies an interface which connects the velocities and will be described below. In the first layer we take advantage of the explicit integration along the vertical, in the second we take into account the viscosity in the vertical direction, hence we recover some friction in the integrated equations. This section is devoted to the study of the viscous layer.

We introduce a small parameter $\overline{\delta}$, whose magnitude will be specified below. It is related to the thickness of the viscous layer, but does not correspond to its actual physical value. We follow the classical strategy used in the so-called boundary layer theory, see e.g. [27],[29], except that in that case $\overline{\delta} \to 0$, whereas we keep a finite value here. The first step is to derive a set of equations, sometimes referred to as RNSP (Reduced Navier-Stokes/Prandtl) equations [22]. Since they are yet two-dimensional, the next step consists in writing another equation, by integrating the Prandtl system over the viscous layer height. This leads to the so-called von Kármán equation, where extra unknowns are introduced. To obtain a closed form, some assumptions have to be done on the vertical velocity profile, which are discussed in the last paragraph.

2.1 Prandtl equations

Starting from the Navier-Stokes equations with long wave scaling, we introduce the following change of variables, referred to as the Prandtl shift:

$$t = \bar{t}, \quad x = \bar{x}, \quad y = \bar{\delta}\bar{y} + f_b, \quad p = \bar{p}.$$

As a consequence, we have the relations

$$\partial_y = \frac{1}{\bar{\delta}}\partial_{\bar{y}}, \qquad \partial_x = \partial_{\bar{x}} - \frac{f_b'}{\bar{\delta}}\partial_{\bar{y}}. \tag{2.1}$$

Velocities must be scaled in order to preserve the mass conservation (1.6), which rewrites here

$$\partial_{\bar{x}} u + \partial_{\bar{y}}\left(\frac{v - f_b' u}{\bar{\delta}}\right) = 0.$$

Hence we choose $\overline{u} = u$ and $\overline{v} = \frac{v - f_b' u}{\bar{\delta}}$. The complete Prandtl shift is therefore

$$x = \bar{x}, \quad y = \bar{\delta}\bar{y} + f_b, \quad t = \bar{t}, \quad p = \bar{p}, \qquad \overline{u} = u, \quad \overline{v} = \frac{v - f_b' u}{\bar{\delta}}. \tag{2.2}$$

Then equations (1.6), (1.7), (1.8) and (1.9) become

$$\partial_{\bar{x}}\overline{u} + \partial_{\bar{y}}\overline{v} = 0$$

$$\partial_{\bar{t}}\overline{u} + \overline{u}\partial_{\bar{x}}\overline{u} + \overline{v}\partial_{\bar{y}}\overline{u} = -\partial_{\bar{x}}\overline{p} + \frac{f_b'}{\bar{\delta}}\partial_{\bar{y}}\overline{p} + \frac{1}{\varepsilon Re_h \bar{\delta}^2}\partial_{\bar{y}}^2\overline{u} \tag{2.3}$$

$$\frac{1}{\bar{\delta}}\partial_{\bar{y}}\overline{p} = -\frac{1}{Fr^2} \tag{2.4}$$

$$\overline{u} = \overline{v} = 0 \qquad \text{at} \qquad \bar{y} = 0.$$

Equation (2.3) together with (2.4) leads to

$$\frac{1}{\varepsilon Re_h \bar{\delta}^2}\partial_{\bar{y}}^2\overline{u} = O(1).$$

This leads to several possible scalings for $\bar{\delta}$ in terms of εRe_h, namely

- if $\bar{\delta}$ verifies $\varepsilon Re_h \bar{\delta}^2 \gg 1$, we recover the ideal fluid equations;
- if $\bar{\delta}$ satisfies $\varepsilon Re_h \bar{\delta}^2 \ll 1$, we obtain $\partial_{\bar{y}}^2\overline{u} = 0$. This equation is explicitly solved and from the continuity of the stress tensor and the adherence on the ground we obtain $u \equiv 0$. So we do not consider this trivial case;
- the last possibility is $\varepsilon Re_h \bar{\delta}^2 \sim 1$. This analysis preserves as many as possible terms in the equations, and hence most of the physical phenomena described by those terms. It is referred to as "dominant balance".

This is why in what follows, we consider the scaling

$$\bar{\delta} = \frac{1}{\sqrt{\varepsilon Re_h}}. \tag{2.5}$$

With this hypothesis, we obtain the Prandtl equations written in viscous layer variables:

$$\begin{cases} \partial_{\bar{x}}\overline{u} + \partial_{\bar{y}}\overline{v} = 0 & (2.6) \\ \partial_{\bar{t}}\overline{u} + \overline{u}\partial_{\bar{x}}\overline{u} + \overline{v}\partial_{\bar{y}}\overline{u} = -\partial_{\bar{x}}\overline{p} - \dfrac{f_b'}{Fr^2} + \partial_{\bar{y}}^2\overline{u} & (2.7) \\ \partial_{\bar{y}}\overline{p} = -\dfrac{\bar{\delta}}{Fr^2} & (2.8) \\ \overline{u} = \overline{v} = 0 \qquad \text{when } \ \bar{y} = 0 & (2.9) \end{cases}$$

Remark 2.1. *The Prandtl equations we obtain are in the same form as those obtained directly with a boundary layer scaling on the Navier-Stokes equations ([29], ch. VII) except for the topography term in* (2.7).

Remark 2.2. *Notice that* (2.8) *implies that* $\partial_{\overline{x}}\overline{p}$ *in* (2.7) *does not depend on* $\overline{y}$.

Up to now, we do not have enough boundary conditions for the viscous layer. The natural connection consists in assuming that the velocity at the "top" of the viscous layer, that is for $\bar{y} = (\eta - f_b)/\overline{\delta}$, coincides with the ground velocity for the ideal fluid, defined by $U_e(t,x) = \big(u_e(t,x), v_e(t,x)\big) = \mathbf{U}\big(t,x,f_b(x)\big)$, where $\mathbf{U} = (u,v)$ is the velocity vector for the ideal fluid. More precisely, we impose the required boundary condition at infinity as

$$\overline{u}\big(t,x,(\eta-f_b)/\overline{\delta}\big) = u_e(t,x), \qquad \overline{\delta}\overline{v}\big(t,x,(\eta-f_b)/\overline{\delta}\big) = v_e(t,x) - f_b'(x)u_e(t,x). \tag{2.10}$$

This is meaningful since in the Prandtl shift $\bar{x} = x$ and $\bar{t} = t$. Note that in classical boundary layer theory the limit known as "asymptotic matching" is used: $\bar{u}(t,x,\bar{y}\to\infty) \to u_e(t,x)$.

Therefore we conclude this paragraph by giving the behaviour of u_e, which is an easy consequence of equations (1.13) and (1.16).

Proposition 2.3. *The horizontal component* u_e *satisfies the following equation:*

$$\partial_t u_e + u_e\partial_x u_e = -\partial_x p|_{y=f_b(x)} \tag{2.11}$$

2.2 Von Kármán equation

The von Kármán equation (see Schlichting [29]) expresses the defect of velocity between the ideal fluid and the viscous layer. A classical way to obtain such an equation consists in writing the Prandtl equation, then introducing the velocity defect $(u_e - \overline{u})$, and finally integrating it on the viscous layer. Following [29] we introduce the following two integrated quantities.

Definition 2.4. *Let* U *be the averaged velocity (Definition 1.4). We define*

- *the displacement thickness* δ_1*, defined by*

$$hU = (h - \overline{\delta}\delta_1)u_e \tag{2.12}$$

- *the momentum thickness* δ_2*, defined by*

$$\int_{f_b}^{\eta} u^2\,dy = \big(h - \overline{\delta}(\delta_1+\delta_2)\big)u_e^2 \tag{2.13}$$

The displacement thickness expresses the distance by which the ground should be displaced to obtain an ideal fluid with velocity u_e with the flow rate hU. In the same way, the momentum thickness accounts for the loss of momentum in the viscous layer.

A simple computation leads to the following expressions for these quantities:

$$\delta_1 = \int_0^{(\eta-f_b)/\delta}\left(1-\frac{\bar{u}}{u_e}\right)d\bar{y}, \qquad \delta_2 = \int_0^{(\eta-f_b)/\delta}\frac{\bar{u}}{u_e}\left(1-\frac{\bar{u}}{u_e}\right)d\bar{y}.$$

Thus we can recover the classical formulæ in the boudary layer scaling $\delta \to 0$ (see [29])

$$\delta_1 = \int_0^{+\infty}\left(1-\frac{\bar{u}}{u_e}\right)d\bar{y}, \qquad \delta_2 = \int_0^{+\infty}\frac{\bar{u}}{u_e}\left(1-\frac{\bar{u}}{u_e}\right)d\bar{y}.$$

Proposition 2.5. *The displacement and momentum thicknesses are ruled by the so-called von Kármán equation:*

$$\partial_t(u_e\delta_1) + u_e\delta_1\partial_x u_e + \partial_x(u_e^2\delta_2) = \tau, \tag{2.14}$$

where $u_e(t,x) = u\big(t,x,f_b(t,x)\big)$ *and* τ *denotes the parietal constraints:*

$$\tau = \partial_{\overline{y}}\overline{u}|_{\overline{y}=0}. \tag{2.15}$$

Remark 2.6. *Notice that in this single equation three new unknowns are actually introduced, namely δ_1, δ_2 and τ. We postpone the presentation of the closure assumptions until the next section.*

Proof. First we notice that (2.11) together with the Prandtl shift rewrites

$$\partial_{\bar t}\overline{u}_e + \overline{u}_e\partial_{\bar x}\overline{u}_e = -\partial_{\bar x}\overline{p}|_{\overline{y}=0} + \frac{f_b'}{\bar\delta}\partial_{\overline{y}}\overline{p}|_{\overline{y}=0} = -\partial_{\bar x}\overline{p} - \frac{f_b'}{Fr^2},$$

where we have used (2.8) to rewrite the right-hand side. The difference between this equation and (2.7) gives

$$\partial_{\bar t}(\overline{u}_e - \overline{u}) + \overline{u}_e\partial_{\bar x}\overline{u}_e - \overline{u}\partial_{\bar x}\overline{u} - \overline{v}\partial_{\overline{y}}\overline{u} = -\partial^2_{\overline{y}}\overline{u}.$$

Through (2.6) and (2.9), we can rearrange the term $\overline{v} = -\int_0^{\overline{y}}\partial_{\bar x}\overline{u}$. Furthermore with the addition and withdrawal of $\overline{u}\partial_{\bar x}\overline{u}_e$, we get

$$\partial_{\bar t}(\overline{u}_e - \overline{u}) + (\overline{u}_e - \overline{u})\partial_{\bar x}\overline{u}_e + \overline{u}\partial_{\bar x}(\overline{u}_e - \overline{u}) + \partial_{\overline{y}}\overline{u}\int_0^{\overline{y}}\partial_{\bar x}\overline{u}\,d\overline{y} = -\partial^2_{\overline{y}}\overline{u}.$$

The last term in the left-hand side is rewritten

$$\partial_{\overline{y}}\overline{u}\int_0^{\overline{y}}\partial_{\bar x}\overline{u}\,d\overline{y} = -\overline{u}\partial_{\bar x}\overline{u} + \partial_{\overline{y}}\left(\overline{u}\int_0^{\overline{y}}\partial_{\bar x}\overline{u}\,d\overline{y}\right).$$

Now we integrate over $\overline{y}$ the resulting equation between 0 and $(\eta - f_b)/\bar\delta$ using the boundary condition (2.10):

$$\begin{aligned}\partial_{\bar t}\left(\int_0^{(\eta-f_b)/\delta}(\overline{u}_e - \overline{u})\,d\overline{y}\right) + \partial_{\bar x}\overline{u}_e\int_0^{(\eta-f_b)/\delta}(\overline{u}_e - \overline{u})\,d\overline{y}&\\ + \int_0^{(\eta-f_b)/\delta}\overline{u}\partial_{\bar x}(\overline{u}_e - \overline{u})\,d\overline{y} - \int_0^{(\eta-f_b)/\delta}\overline{u}\partial_{\bar x}\overline{u}\,d\overline{y} + u_e\int_0^{(\eta-f_b)/\delta}\partial_{\bar x}\overline{u}\,d\overline{y}&\\ = \partial_{\overline{y}}\overline{u}|_{\overline{y}=0}.&\end{aligned}$$

The last three terms of the left-hand side can be rewritten as $\partial_{\bar x}\left(\int_0^{(\eta-f_b)/\delta}\overline{u}(\overline{u}_e - \overline{u})\,d\overline{y}\right)$. So, using also definition (2.15), the equation becomes:

$$\partial_{\bar t}\left(\int_0^{(\eta-f_b)/\delta}(\overline{u}_e - \overline{u})\,d\overline{y}\right) + \partial_{\bar x}\overline{u}_e\int_0^{(\eta-f_b)/\delta}(\overline{u}_e - \overline{u})\,d\overline{y} + \partial_{\bar x}\left(\int_0^{(\eta-f_b)/\delta}\overline{u}(\overline{u}_e - \overline{u})\,d\overline{y}\right) = \tau.$$

Finally, since u_e is independent of $\overline{y}$, we have the relations

$$u_e\delta_1 = \int_0^{(\eta-f_b)/\delta}(u_e - \overline{u})\,d\overline{y}, \qquad u_e^2\delta_2 = \int_0^{(\eta-f_b)/\delta}\overline{u}(u_e - \overline{u})\,d\overline{y},$$

and since all the unknowns are independent of $\overline{y}$ and $t = \bar t$, we can drop as well the bars in the derivatives. With all this, we obtain equation (2.14). □

2.3 Velocity profile in the viscous layer

The von Kármán equation (2.14) together with the equation on u_e (2.11) give only a partial representation of the boundary layer, since they involve four unknowns, namely u_e, δ_1, δ_2, and $\partial_{\overline{y}}\overline{u}|_{\overline{y}=0}$ which represents the parietal forces. To proceed further towards an integrated model, we need a closure for this system of equations. By definition, the viscous layer is the layer where the velocity $\overline{u}$ varies from 0 on the floor to u_e. Therefore we introduce a profile function φ as well as a scaling factor $\Delta(\bar t, \bar x)$, chosen in such a way that Δ quantifies the physical thickness of the viscous layer. As a general rule we wish to have

$$\frac{\overline{u}(\overline{y})}{u_e} = \varphi\left(\frac{\overline{y}}{\Delta(\bar t, \bar x)}\right) = \varphi(\zeta).$$

Therefore we choose $\Delta \leq (\eta - f_b)/\overline{\delta}$, and φ such that

$$\varphi(\overline{t},\overline{x},0) = 0, \qquad \varphi(\overline{t},\overline{x},\overline{y}) = 1 \quad \text{when } \Delta \leq \overline{y} \leq (\eta - f_b)/\overline{\delta}, \qquad \int_0^1 (1-\varphi)\, d\zeta \equiv \alpha_2 < +\infty. \tag{2.16}$$

Hence

$$\delta_1 = \int_0^{(\eta-f_b)/\overline{\delta}} \left(1 - \frac{\overline{u}(\overline{y})}{u_e}\right) d\overline{y} = \int_0^{(\eta-f_b)/\overline{\delta}} \left(1 - \varphi\big(\overline{y}/\Delta\big)\right) d\overline{y} = \Delta\alpha_2.$$

Therefore choosing Δ amounts to fixing the form factor α_2 defined in (2.16) (e.g. $\Delta = \delta_1$ corresponds to $\alpha_2 = 1$). Now we can readily obtain a relationship between δ_1 and δ_2:

$$\delta_2 = \Delta \int_0^{(\eta-f_b)/\overline{\delta}} \varphi(1-\varphi)\, d\zeta = \frac{\delta_1}{H}, \qquad \text{where} \quad \alpha_1 = \int_0^1 \varphi(1-\varphi)\, d\zeta \quad \text{and} \quad H = \frac{\alpha_2}{\alpha_1}. \tag{2.17}$$

Finally, the parietal constraints can also be expressed in terms of the profile φ:

$$\tau = \partial_{\overline{y}}\overline{u}|_{\overline{y}=0} = \frac{u_e}{\Delta}\varphi'(0) = \frac{u_e\alpha_2}{\delta_1}\varphi'(0). \tag{2.18}$$

The collection of all the preceding relations leads to put the Von Kármán equation (2.14) on the following form:

$$\partial_t(u_e\delta_1) + u_e\delta_1\partial_x u_e + \partial_x(\frac{u_e^2\delta_1}{H}) = \frac{u_e\alpha_2}{\delta_1}\varphi'(0). \tag{2.19}$$

At this stage, several shapes can be used for the profile, including turbulent ones. As far as laminar profiles are concerned, we refer to [29, ch.X] for elements of comparisons between different profiles. According to the velocity profile similarity principle over a flat plane at zero-incidence [29], we shall assume that φ depends solely on the ζ variable. Table 1 contains the results for two polynomials approximations: the piecewise linear one and the parabolic one. These two profiles do not allow the observation of separation for decelerated flows as their coefficients are fixed. Adaptive profiles allowing flow separation can also be seen, for instance in [5] for the Integral Interacting Boundary Layer equations (IBL).

Velocity distribution ($0 \leqslant \zeta \leqslant 1$)	α_2	H	$\varphi'(0)$
$\varphi(\zeta) = \zeta$	1/2	3	1
$\varphi(\zeta) = -\zeta^2 + 2\zeta$	1/3	5/2	2

Table 1: Piecewise linear and parabolic profiles for a finite layer $\overline{\delta}\Delta$. Note that for an infinite layer, the solution would be Blasius solution where $\alpha_2\varphi'(0) = 0.332$ and $H = 2.59$. See Schlichting for other possible choices.

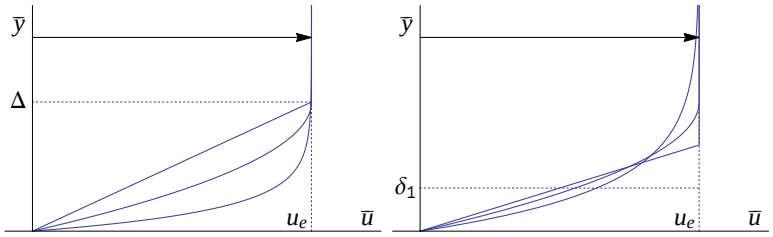

Figure 2: Left, three examples of test velocity profiles : from top to bottom a piecewise linear profile up to a finite Δ, a parabolic profile up to a finite Δ, a Blasius like profile. Right the same profiles are plotted for a same δ_1 focusing on the displacement thickness (2.12).

Remark 2.7.

- *In the case where $u \leq u_e$, the shape factor H satisfies $H \geq 1$ since $\alpha_1 \leq \alpha_2$.*
- *The limit case $H = 1$ enforces a discontinuity at the origin for φ: $\varphi \equiv 1$ for $\zeta > 0$, $\varphi(0) = 0$, thus formally leading to a singular friction term in the equation.*

3 Extended shallow water model

We are now in position to obtain the extended model we are looking for. The first step consists in integrating the mass and momentum conservation equations, as in the usual way to derive the shallow water equations from Navier-Stokes, see for instance [15]. The resulting mass equation is the same, but several differences occur for momentum. Indeed, the parietal constraints arise in the right-hand side at order 1 in $\overline{\delta}$, motivating a new closure for the momentum flux. The momentum equation thus depends on the unknowns δ_1 and δ_2, so the system has to be coupled with the von Kármán equation we derived above.

3.1 Mass and momentum integrated equations

We recall that the natural averaged velocity in viscous shallow water is $hU = \int_{f_b}^{\eta} u\,dy$. From the incompressibility equations we recover the usual balance equation on the water depth h.

Proposition 3.1 (Mass equation)**.** *The mass conservation in its integrated form is*

$$\partial_t h + \partial_x(hU) = 0. \tag{3.1}$$

Proof. We integrate the conservation equation (1.6) between f_b and η

$$\begin{aligned} v(t,x,\eta) &= v(t,x,f_b) - \int_{f_b}^{\eta} \partial_x u\,dy \\ &= v(t,x,f_b) - \partial_x\left(\int_{f_b}^{\eta} u\,dy\right) + u(t,x,\eta)\partial_x\eta - u(t,x,f_b)f_b'. \end{aligned}$$

Now from the no-slip boundary condition (1.9) we get $v(t,x,f_b) = u(t,x,f_b) = 0$, and the kinematic one (1.10) gives $u(t,x,\eta)\partial_x\eta - v(t,x,\eta) = -\partial_t\eta = -\partial_t h$ since the ground is independent of time, and we recognize (3.1). □

We turn now to the momentum balance equation. The main point to notice at this stage is the appearance of the parietal constraint τ with prefactor $\overline{\delta}$.

Proposition 3.2 (Momentum equation)**.** *The integrated momentum conservation is written:*

$$\partial_t(hU) + \partial_x\left(\int_{f_b}^{\eta} u^2\,dy\right) = -h\partial_x p - \overline{\delta}\tau, \tag{3.2}$$

where τ is defined by (2.15)*.*

Proof. We apply the same process as for the equation of mass conservation. Recall that the momentum equation (1.7) together with the scaling (2.5) can be rewritten

$$\partial_t u + u\partial_x u + v\partial_y u = -\partial_x p + \overline{\delta}^2\partial_y^2 u.$$

We integrate in y, and recall that $\partial_x p$ does not depend on y, see Remark 2.2. Hence we get

$$\int_{f_b}^{\eta} \partial_t u + \int_{f_b}^{\eta} u\partial_x u\,dy + \int_{f_b}^{\eta} v\partial_y u\,dy = -h\partial_x p + \int_{f_b}^{\eta} \overline{\delta}^2\partial_y^2 u\,dy.$$

Exchanging the time derivative and the integral, and integrating by parts in the last term of the left-hand side gives

$$\partial_t\left(\int_{f_b}^{\eta} u\,dy\right) - u(t,x,\eta)\partial_t\eta + \int_{f_b}^{\eta} u\partial_x u\,dy + [vu]_{f_b}^{\eta} - \int_{f_b}^{\eta} u\partial_y v\,dy = -h\partial_x p - \overline{\delta}^2\partial_y u|_{y=f_b}$$

Finally we use the mass conservation (1.1) to replace the $\partial_y v$ term, and the parietal force is estimated thanks to the Prandtl shift, since $\partial_y u|_{y=f_b} = \partial_{\bar{y}}\bar{u}|_{\bar{y}=0}/\overline{\delta} = \tau/\overline{\delta}$ (see (2.15) above). Therefore we obtain

$$\partial_t\left(\int_{f_b}^{\eta} u\,dy\right) - u(t,x,\eta)\partial_t\eta + \int_{f_b}^{\eta} 2u\partial_x u\,dy + [vu]_{f_b}^{\eta} = -h\partial_x p - \overline{\delta}\tau,$$

which together with the boundary conditions gives (3.2). □

Remark 3.3. *Both equations* (3.1) *and* (3.2) *remain true for an ideal fluid as well, since the terms at* $y = f_b$ *cancel thanks to the non penetration boundary condition* (1.16).

Remark 3.4. *The viscous layer theory leads to a friction term in a laminar form but only over the height* $\overline{\delta}\delta_1$. *Also the order term is only* $\overline{\delta}$ *whereas for the Poiseuille-shallow water (see equation (1.22)) it is at order* $\overline{\delta}^2 = \frac{1}{\varepsilon Re}$.

3.2 Towards the extended model

At this point we are faced with two equations (3.1) and (3.2) which are very similar to the usual shallow water equations, except that the friction term is not given explicitly in terms of U and/or h. A consistent expression with the model is obtained through the velocity profile, see (2.18) above. The momentum equation remains unclosed: we need to give a closure for $\int_{f_b}^{\eta} u^2\,dy$. The classical approximation for the shallow water system is based on the fact that for an ideal fluid with a low depth, we have $\int_{f_b}^{\eta} u_{PF}^2\,dy \simeq \frac{1}{h}\left(\int_{f_b}^{\eta} u_{PF}\,dy\right)^2$ as we said in section 1.3.

Relation (2.13) does not give any closure for the momentum flux, it merely emphasizes that it can be entirely completed by the choice of δ_2. In this respect, we prove now that this expression for the flux is the most convenient, since it takes into account the effect of the viscous layer, and in some sense independantly of the choice for δ_2. The complete closure can be achieved by the study of the viscous layer, as we did above in Section 2.3. More precisely, we have the following two results, which clarify the role of the von Kármán equation. The starting point is the system of three integrated equations:

$$\partial_t h + \partial_x(hU) = 0 \tag{3.3}$$

$$\partial_t(hU) + \partial_x J = -h\partial_x p - \overline{\delta}\tau \tag{3.4}$$

$$\partial_t u_e + u_e\partial_x u_e = -\partial_x p, \tag{3.5}$$

where J is the momentum flux for which we seek a closure. We evidence now the fact that a convenient definition of J allows to recover the von Kármán equation from this system of integrated equations.

Proposition 3.5. *Let* (h, U, u_e, J) *be solution to* (3.3), (3.4) *and* (3.5). *Assume* δ_1 *is defined by* (2.12). *Then* δ_1 *and* δ_2 *solve the von Kármán equation* (2.14) *if and only if there holds*

$$J = \big(h - \overline{\delta}(\delta_1 + \delta_2)\big)u_e^2. \tag{3.6}$$

Proof. We start from the von Kármán equation and introduce (2.12) to obtain

$$\partial_t(hu_e) - \partial_t(hU) + (hu_e - U)\partial_x u_e + \overline{\delta}\partial_x(u_e^2\delta_2) = \overline{\delta}\tau.$$

To this equation we add (3.4), the parietal term disappears, leading to

$$\partial_t(hu_e) + \partial_x J + hu_e\partial_x u_e - hU\partial_x u_e + \overline{\delta}\partial_x(u_e^2\delta_2) = -h\partial_x p.$$

Developping the time derivative and simplifying with (3.5) we obtain

$$u_e\partial_t h + \partial_x J - hU\partial_x u_e + \partial_x\big(\overline{\delta}u_e^2\delta_2\big) = 0.$$

Finally, we use (3.3) to eliminate the time derivative, regroup terms and get

$$\partial_x\big(J - hu_eU + \overline{\delta}\delta_2 u_e^2\big) = 0,$$

so that, up to a constant which can be taken equal to zero by considering that the flux is zero when the velocity is zero, we have

$$J = hu_eU - \overline{\delta}\delta_2 u_e^2, \tag{3.7}$$

which together with (2.12) gives precisely (3.6).

Conversely, we consider (2.12) and use successfully the mass and momentum balance equations

$$\begin{aligned}
\partial_t(u_e\overline{\delta}\delta_1) &= \partial_t(hu_e) - \partial_t(hU) = u_e\partial_t h + h\partial_t u_e + \partial_x\big(\big(h - \overline{\delta}(\delta_1+\delta_2)\big)u_e^2\big) + h\partial_x p + \overline{\delta}\tau\\
&= -u_e\partial_x(hU) - hu_e\partial_x u_e - h\partial_x p + \partial_x(hu_e^2) - \overline{\delta}\partial_x\big((\delta_1+\delta_2)u_e^2\big) + h\partial_x p + \overline{\delta}\tau\\
&= -u_e\partial_x(hu_e) + u_e\partial_x(\overline{\delta}\delta_1 u_e) - hu_e\partial_x u_e + \partial_x(hu_e^2) - \overline{\delta}\partial_x\big((\delta_1+\delta_2)u_e^2\big) + \overline{\delta}\tau\\
&= -\overline{\delta}\left(-u_e\partial_x(\delta_1 u_e) + \partial_x((\delta_1+\delta_2)u_e^2) - \tau\right).
\end{aligned}$$

Noting that $\partial_x(\delta_1 u_e^2) = u_e\partial_x(\delta_1 u_e) + \delta_1 u_e\partial_x u_e$ we recover as required the von Kármán equation. □

In the above proposition, we only use the three equations (3.3)-(3.5) and the physical definition (2.12) of δ_1. However if we forget the physical definition, we obtain another formulation using the von Kármán equation (2.14) together with equations (3.3)-(3.5). This approach gives back the physical definition in the sense of characteristics as explained in the next proposition.

Proposition 3.6. *Let J be defined by* (3.6)*, and (h, U, δ_1, u_e) be a (smooth) solution to the system* (3.3)*,* (3.4)*,* (3.5)*, together with the von Kármán equation* (2.14)*. Denote by δ_1^* the thickness obtained using* (2.12)*. Then*

$$\partial_t \left(u_e(\delta_1 - \delta_1^*)\right) - u_e \partial_x \left(u_e(\delta_1 - \delta_1^*)\right) = 0.$$

Hence, the error is constant along the characteristics of the ideal fluid. In particular, if initially $\delta_1 = \delta_1^*$ then it is true for all times.

Proof. From (2.12)

$$\begin{aligned}
\partial_t(u_e\overline{\delta}\delta_1^*) &= \partial_t(hu_e) - \partial_t(hU) = u_e\partial_t h + h\partial_t u_e + \partial_x\big(\big(h - \overline{\delta}(\delta_1+\delta_2)\big)u_e^2\big) + h\partial_x p + \overline{\delta}\tau \\
&= -u_e\partial_x(hU) - hu_e\partial_x u_e - h\partial_x p + \partial_x(hu_e^2) - \overline{\delta}\partial_x\big((\delta_1+\delta_2)u_e^2\big) + h\partial_x p + \overline{\delta}\tau \\
&= -u_e\partial_x(hu_e) + u_e\partial_x(\overline{\delta}\delta_1^* u_e) - hu_e\partial_x u_e + \partial_x(hu_e^2) - \overline{\delta}\partial_x\big((\delta_1+\delta_2)u_e^2\big) + \overline{\delta}\tau \\
&= -\overline{\delta}\left(-u_e\partial_x(\delta_1^* u_e) + \partial_x((\delta_1+\delta_2)u_e^2) - \tau\right).
\end{aligned}$$

Now using the von Kármán equation to eliminate δ_2, we obtain

$$\begin{aligned}
\overline{\delta}\partial_t(u_e\delta_1^*) &= -\overline{\delta}\left(-u_e\partial_x(\delta_1^* u_e) + \partial_x(\delta_1 u_e^2) - \partial_t(u_e\delta_1) - u_e\delta_1\partial_x u_e\right) \\
&= -\overline{\delta}\left(-u_e\partial_x\big(u_e(\delta_1^* - \delta_1)\big) - \partial_t(u_e\delta_1)\right),
\end{aligned}$$

which is the desired result. □

3.3 Final Extended shallow water model

In summary, putting together the results of Proposition 3.5, the closure formulas (2.18) and (2.17) using the velocity profile in the viscous layer, and the hydrostatic law for the pressure (1.8), we obtain a system of three partial differential equations, repectively for the mass conservation, the momentum conservation, and the behaviour of the prefect fluid, namely

$$\begin{cases}
\partial_t h + \partial_x(hU) = 0 & (3.8)\\
\partial_t(hU) + \partial_x\left(\dfrac{h^2}{2Fr^2} + \big(h - \bar{\delta}\delta_1(1+\dfrac{1}{H})\big)u_e^2\right) = -\dfrac{hf_b'}{Fr^2} - \overline{\delta}\dfrac{u_e\alpha_2}{\delta_1}\varphi'(0) & (3.9)\\
\partial_t u_e + u_e\partial_x u_e = -\dfrac{1}{Fr^2}(\partial_x h + f_b') & (3.10)
\end{cases}$$

Propositions 3.5 and 3.6 show that there are two equivalent possibilities to compute δ_1 in order to close the system. The first one consists in adding the algebraic relation (2.12), which gives somewhat an equation of state:

$$hU = (h - \bar{\delta}\delta_1)u_e. \tag{3.11}$$

The second one makes use of the von Kármán equation, so that δ_1 appears as another conserved quantity

$$\partial_t(u_e\delta_1) + u_e\delta_1\partial_x u_e + \partial_x(\frac{u_e^2\delta_1}{H}) = \frac{u_e\alpha_2}{\delta_1}\varphi'(0). \tag{3.12}$$

The relations between h, U, u_e and δ_1 through the displacement thickness (2.12) and (2.13) directly imply the following expressions for the momentum flux

$$\int_{f_b}^{\eta} u^2\,dy = (h - \bar{\delta}(\delta_1+\delta_2))u_e^2 = \frac{\big(h - \overline{\delta}(\delta_1+\delta_2)\big)U^2}{(1-\overline{\delta}\delta_1/h)^2} = hU^2 + \overline{\delta}(\delta_1 - \delta_2 - \overline{\delta}\delta_1^2/h)u_e^2. \tag{3.13}$$

The last one, which can be rewritten as a ratio of fluxes:

$$\frac{h\int u^2\,dy}{(\int u^2\,dy)^2} = 1 + \overline{\delta}\frac{(\delta_1 - \delta_2 - \overline{\delta}\delta_1^2/h)u_e^2}{hU^2}, \tag{3.14}$$

enhances the extension of the classical shallow water model without friction: taking abruptly $\overline{\delta} = 0$ in these equations, the first two equations are decoupled from the last one and we recover the classical momentum equation (1.19) (with a ratio equal to one). On the other hand, as soon as viscosity effects arise, that is $\overline{\delta} > 0$, we have not only the friction term on the right-hand side but also a correction of order one in $\overline{\delta}$ to the hydrostatic pressure. This is consistent with the order of magnitude of the friction term. In [14] a similar correction in the flux of the shallow water system is proposed to improve the study of roll-waves.

In the following, we choose to compute the model with the equations (3.8), (3.9), (3.10) and (3.12) instead of (3.8), (3.9), (3.10) and (3.11). Indeed the equation (3.12) gives more information about the evolution of the displacement thickness (see part 4). Furthermore this choice is more stable for the illustrations in Section 5.

From now, we limit ourselves to a constant shape for the velocity profile in the viscous layer (piecewise linear or parabolic, see table 1) which expresses by the form parameter H and the shear stress $\varphi'(0)$ constants in the equations (3.9) and (3.12).

Remark 3.7. *An aerodynamic type approach would not conserve the equation (3.9) but instead (3.8), (3.10), (3.11) and (3.12). Equation (3.9) is the important point of this work which combines the aerodynamic approach and the shallow water one. Furthermore, this approach is known as "Interactive Boundary Layer" or "Viscous Inviscid Interaction" in aerodynamics [24].*

4 Examples of explicit solutions

We present in this section several analytical solutions which can be used for testing the numerical methods. First we provide two solutions to the von Kármán equation, for short and long times, then a solution to the complete linearized problem. The few simulations of the ESW model in this part are obtained with the numerical scheme presented in Section 5.

4.1 Blasius solution to the von Kármán equation

In this part, we consider the von Kármán equation in the following configuration, also studied by Stewartson [31, Sec. 3]:

- u_e is constant,
- $f_b = 0$,
- H, $\varphi'(0)$ are constant.

Consequently the von Kármán equation (3.12) can be rewritten

$$\partial_t(\delta_1^2) + \frac{u_e}{H}\partial_x(\delta_1^2) = 2\alpha_2\varphi'(0), \quad x \in \mathbb{R}^+,\, t \in \mathbb{R}^+, \tag{4.1}$$

and it has to be complemented with the following initial and boundary value conditions:

$$\delta_1^2(0,x) = b_0(x), \quad x \in \mathbb{R}^+, \qquad \delta_1^2(t,0) = b_1(t), \quad t \in \mathbb{R}^+. \tag{4.2}$$

The solution is readily obtained by the method of characteristics:

$$\delta_1(t,x) = \begin{cases} \sqrt{b_1(t - \frac{H}{u_e}x) + \frac{2\alpha_2 H}{u_e}\varphi'(0)x} & \text{if} \quad x \le \frac{u_e t}{H} \\ \sqrt{b_0(x - \frac{u_e}{H}t) + 2\alpha_2\varphi'(0)t} & \text{if} \quad x > \frac{u_e t}{H} \end{cases} \tag{4.3}$$

It is clear on this formula that for t large enough the initial value of δ_1 has no influence on the solution. Figure 3 illustrates the creation and development of the viscous layer, with initial and boundary values $b_0 \equiv b_1 \equiv 0$ and $u_e \equiv 1$. When time evolves, $\delta_1(t,x)$ captures indeed the Blasius solution $\sqrt{\frac{2\alpha_2 H}{u_e}\varphi'(0)x}$. Notice that this solution of the von Kármán equation with constant u_e creates an unbounded viscous layer, without regards of the limitation of the water depth. Hence it is clearly physically not valid for large x or t. In this context, a final time $T = 3$ is enough to get the profile all over the domain $[0,1]$.

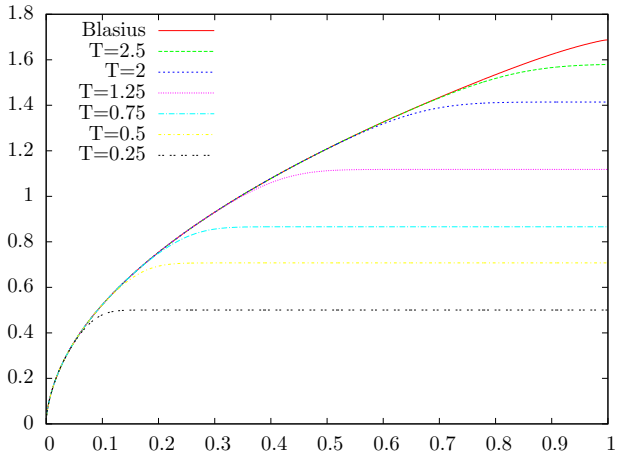

Figure 3: Time evolution of δ_1. Linear velocity profile ($\alpha_2 = \frac{1}{2}$, $H = 3$, $\varphi'(0) = 1$), $u_e \equiv 1$, final time $T = 3$; $\bar{\delta} = 10^{-\frac{9}{2}}$

4.2 Steady state for the von Kármán equation

We turn now to the study of the von Kármán equation with the aerodynamic point of view (see remark 3.7) for large times. More precisely we assume that δ_1 is stationary, similar to the Interactive Boundary Layer in [5]. Then equation (3.12) becomes

$$\partial_x \delta_1 + (2+H)\frac{\partial_x u_e}{u_e}\delta_1 = \frac{H\alpha_2\varphi'(0)}{u_e\delta_1}.$$

If we assume in addition that both h and U are constant, combined with the relation $u_e = \frac{hU}{h-\bar{\delta}\delta_1}$, we recover

$$\partial_x u_e = u_e \frac{\bar{\delta}\partial_x\delta_1}{h-\bar{\delta}\delta_1}.$$

Then, the large time von Kármán equation is an ordinary differential equation in δ_1:

$$\partial_x \delta_1 = \frac{H\alpha_2\varphi'(0)(h-\bar{\delta}\delta_1)}{hU\delta_1[1+(2+H)\frac{\bar{\delta}\delta_1}{h-\bar{\delta}\delta_1}]}. \tag{4.4}$$

Equation (4.4) is consistent with the the Blasius solution (4.3) when $\bar{\delta}$ goes to 0 and $u_e = U$. This corresponds to a small value of the effective displacement thickness $\bar{\delta}\delta_1$, hence to small values of x. Figure 4 displays the three solutions we have at hand, and clearly evidences this behaviour.

On the other hand, equation (4.4) exhibits a stationary solution $\bar{\delta}\delta_1 = h$, and we observe indeed a saturation for large values of x, see Figure 5. Notice also that the smaller $\bar{\delta}$ is, the larger is the domain size required to reach the stationary state. Hence computing the stationary solution with the complete ESW model may be very difficult. Moreover it is not clear that actual solutions to the complete ESW system satisfy h and U constant for large x, so that, even if such saturation behaviour is physically plausible, this solution definitely might not be caught by the extended model, which can explain the difference in Figure 4.

4.3 Stationary solution on a flat ground

The previous section evidences a steady solution for the displacement thickness for any parameter $\bar{\delta}$ with the assumption that h and U are constant. In this part, we look for a steady form for all the unknowns on a flat ground. This steady form, depending on $\bar{\delta}$, is an explicit non constant solution. It is actually a solution to the linearized system of equations, over a particular steady state.

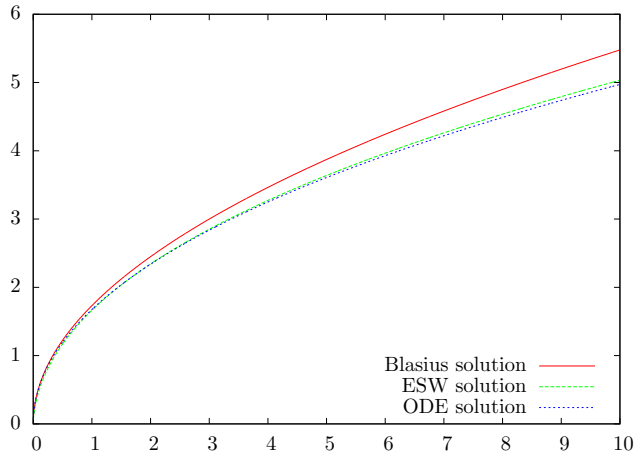

Figure 4: Three computations of δ_1: Blasius (4.3) (red), ODE (4.4) (blue) and full ESW system (green). At the entrance, the ODE as well the ESW solution fit the Blasius one, then they depart from each other. Linear profile ($\alpha_2 = \frac{1}{2}$, $H = 3$, $\varphi'(0) = 1$), $\bar{\delta} = 0.01$, $h = 1$, $U = 1$, initial data $u_e = 1$, $\delta_1 = 0.01$.

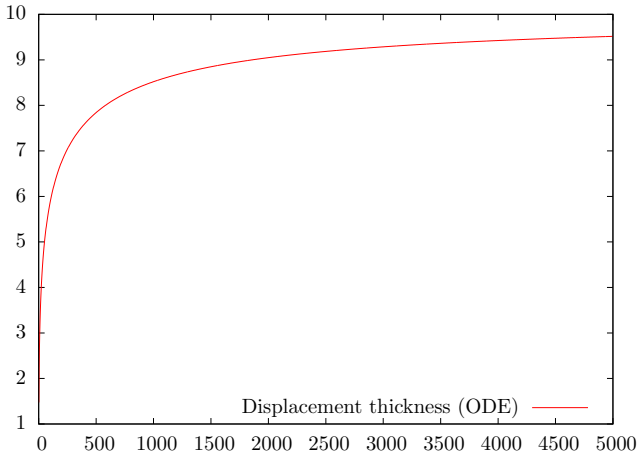

Figure 5: The displacement thickness $\bar{\delta}\delta_1$ computed as a solution of (4.4). Linear profile ($\alpha_2 = \frac{1}{2}$, $H = 3$, $\varphi'(0) = 1$), $\bar{\delta} = 0.1$, $h = 1$ and $U = 1$.

For any unknown function g, we look for an expansion $g = g^0 + \bar{\delta} g^1 + \cdots$, and drop all terms of order greater than 2. We start from the steady equations, in their aerodynamics-like form (see remark 3.7):

$$\partial_x(hU) = 0 \tag{4.5}$$

$$u_e \delta_1 \partial_x u_e + \partial_x(u_e^2 \frac{\delta_1}{H}) = \frac{u_e \alpha_2 \varphi'(0)}{\delta_1} = \tau \tag{4.6}$$

$$u_e \partial_x u_e = -\frac{1}{Fr^2} \partial_x h \tag{4.7}$$

$$hU = (h - \bar{\delta}\delta_1) u_e \tag{4.8}$$

First we notice the decomposition of the two following terms:

$$hU = h^0 U^0 + \bar{\delta}(h^1 U^0 + h^0 U^1)$$

$$(h - \bar{\delta}\delta_1) u_e = h^0 u_e^0 + \bar{\delta}(h^1 u_e^0 + h^0 u_e^1 - \delta_1^0 u_e^0).$$

4.3.1 Order 0 term

This provides us with the required steady state.

1. Thanks to the relation (4.8), $u_e^0 = U^0$;
2. the equations (4.5) and (4.7), written only with h^0 and u_e^0, imply that h^0 and u_e^0 are constants (and so U^0 too);
3. consequently, equation (4.6) becomes
$$(u_e^0)^2 \frac{1}{H} \partial_x(\delta_1^0) = \tau, \tag{4.9}$$
which readily gives δ_1^0:
$$\delta_1^0 = \sqrt{\frac{2\alpha_2 H}{u_e^0}\varphi'(0)}\sqrt{x}.$$

Notice that this expression is valid only if $H \geq 0$ and $\varphi'(0) \geq 0$, which is ensured by the choice of the profile φ.

4.3.2 Order 1 term

We turn now to the order 1 perturbation of the above steady state.

1. With the equation (4.7), we get a relation between u_e^1 and h^1:
$$u_e^0 \partial_x u_e^1 = -\frac{1}{Fr^2}\partial_x h^1; \tag{4.10}$$
2. the combination of the relation (4.8) and the equation (4.5) we have
$$u_e^0 \partial_x h^1 + h^0 \partial_x u_e^1 - u_e^0 \partial_x \delta_1^0 = 0.$$
Introducing in this expression the relation (4.10), we get
$$\partial_x u_e^1 = \frac{u_e^0}{h^0 - (u_e^0)^2 Fr^2}\partial_x \delta_1^0.$$
Integrating in x, we get an explicit form for u_e^1 in terms of δ_1^0:
$$u_e^1 = \frac{u_e^0}{h^0}\frac{1}{1 - Fr_0^2}\delta_1^0.$$
where Fr_0 is the local Froude number defined by $\frac{U^0}{\sqrt{\frac{1}{Fr^2}h^0}}$.
3. Thanks to the equation (4.10) we have
$$h^1 = \frac{u_e^0 Fr^2}{h^0}\frac{1}{Fr_0^2 - 1}\delta_1^0.$$
As $\frac{u_e^0 Fr^2}{h^0} = Fr_0^2$, we finally get
$$h^1 = \frac{Fr_0^2}{Fr_0^2 - 1}\delta_1^0.$$
4. Exploiting the equation (4.5) with h and U, we obtain from the above relation
$$U^1 = \frac{U^0}{h^0}\frac{Fr_0^2}{1 - Fr_0^2}\delta_1^0.$$

So, we have state a linearized non constant solution for the steady system (4.5)-(4.7):

$$\begin{cases} \delta_1^0 = \sqrt{\frac{2\alpha_2 H}{u_e}\varphi'(0)}\sqrt{x} \\ u_e = u_e^0 + \overline{\delta}\frac{U^0}{h^0}\frac{1}{1-Fr_0^2}\delta_1^0 \\ h = h^0 + \overline{\delta}\frac{Fr_0^2}{Fr_0^2-1}\delta_1^0 \\ U = U^0 + \overline{\delta}\frac{U^0}{h^0}\frac{Fr_0^2}{1-Fr_0^2}\delta_1^0. \end{cases} \tag{4.11}$$

5 Numerical illustrations

The aim of this last part is to illustrate in a simple way the behaviours of the different variables of the ESW system. We are aware that more accurate analysis is mandatory to study the system. In a first step, we briefly present the numerical scheme we use. A second step will be devoted to a comparison between the ESW solutions and those of the classical shallow water system (SW). Finally we will observe the evolution of the displacement thickness and the friction term with different parameters of the calculation.

5.1 Numerical scheme

We recall and fix some notations in the general framework of a system of nonlinear conservation laws in the form

$$\partial_t V + \partial_x G(V) = S(t,x,V),$$

where G is the flux and S the source term. Recall that the aim of this part is not to establish a sharp discretization, but merely to illustrate some interesting features of the ESW system. We apply a standard finite volume method with time splitting for the source terms. As regard the conservative equation without the source term we use a first-order explicit three points scheme ([6]):

$$V_i^{n+1} = V_i^n - \frac{\Delta t}{\Delta x}(F_{i+\frac{1}{2}} - F_{i-\frac{1}{2}})$$

where $F_{i+\frac{1}{2}} = F(V_i^n, V_{i+1}^n)$. The choice of the numerical flux F determines the scheme. We choose here a HLL scheme. If we denote by λ_i the eigenvalues of $D_V G(V)$, the flux F, in our notations, is defined by:

$$F(V_l,V_r) = \begin{cases} G(V_l) \quad \text{if} \quad c_1 > 0 \\ \frac{c_2 G(V_l) - c_1 G(V_r) + c_1 c_2 (V_r - V_l)}{c_2 - c_1} \quad \text{if} \quad c_1 \leq 0 \leq c_2 \\ G(V_r) \quad \text{if} \quad c_2 < 0 \end{cases}$$

with $c_1 = \min\limits_{V=V_l,V_r}(\min\limits_i \lambda_i(V))$ and $c_2 = \max\limits_{V=V_l,V_r}(\max\limits_i \lambda_i(V))$.

The pressure term in the equation (3.10) contains a spatial derivate of the water height h. To fully respect the formulation above, this term should be included in $D_V G(V)$. However this leads to a matrix whose eigenvalues are not known and so this complicates the computation. In the following we treat all the pressure term in equation (3.10) as a source term. With this choice and the flux presented in (3.13), $\displaystyle\int_{f_b}^{\eta} u^2\, dy = hU^2 + \bar{\delta}(\delta_1 - \delta_2 - \frac{\bar{\delta}\delta_1^2}{h})u_e^2$, $D_V G(V)$ is a block diagonal matrix whose four eigenvalues can be computed and are comparable with the classical eigenvalues of the shallow water system:

$$U + \sqrt{\frac{h}{Fr^2} + \left(\frac{\bar{\delta}\delta_1 u_e}{h}\right)^2}, \qquad U - \sqrt{\frac{h}{Fr^2} + \left(\frac{\bar{\delta}\delta_1 u_e}{h}\right)^2}, \qquad u_e, \qquad \frac{u_e}{H}. \tag{5.1}$$

The HLL scheme could be computed in this state. Nevertheless, we have not the means to propose an equivalence of the classical hydrostatic reconstruction in order to match the usual simulations when $\bar{\delta} \simeq 0$. As the block diagonal form inspires a possible splitting of the equations without denaturing the global bahavior, we choose to do the computation of the flux in several steps all the while conserving the information of the eigenvalues as regards the speeds used in the HLL scheme.

1. The ideal velocity is firstly computed thanks to the equation (3.10) with only a centered difference for the source term:

   $$(u_e)_i^{n+1} = (u_e)_i^n - \frac{\Delta t}{\Delta x}\left[F_{u_e}((u_e)_i^n, (u_e)_{i+1}^n) - F_{u_e}((u_e)_{i-1}^n, (u_e)_i^n) + \frac{1}{2Fr^2}(h_{i+1}^n - h_{i-1}^n + (f_b)_{i+1} - (f_b)_{i-1})\right].$$

   where F_{u_e} is linked to $G_{u_e}(v) = \frac{v^2}{2}$

2. Let $w = u_e\delta_1$. The von Kármán equation (3.12) gives:

   $$w_i^{n+1} = w_i^n - \frac{\Delta t}{\Delta x}\left(F_{VK}(w_i^n, w_{i+1}^n) - F_{VK}(w_{i-1}^n, w_i^n) + \frac{w_i^n}{2}((u_e)_{i+1}^{n+1} - (u_e)_{i-1}^{n+1})\right) + \Delta t \frac{((u_e)_i^{n+1})^2 \alpha_2 \varphi'(0)}{w_i^n}$$

   with F_{VK} associated to $G_{VK}(w) = \frac{u_e}{H}w$.

3. Let $V = \begin{pmatrix} h \\ hU \end{pmatrix}$. The two equations of conservation (3.8)-(3.9) are rewritten in the form:

$$\partial_t V + \partial_x(G_{HR}(V)) + \partial_x \begin{pmatrix} 0 \\ \bar{\delta} u_e^2 \delta_1 (1 - \frac{1}{H}) - \frac{(\bar{\delta} u_e \delta_1)^2}{V_1} \end{pmatrix} = \begin{pmatrix} 0 \\ -\frac{V_1}{Fr^2} f_b' - \bar{\delta} \frac{u_e \alpha_2 \varphi'(0)}{\delta_1} \end{pmatrix}$$

where $G_{HR}(V) = \begin{pmatrix} V_2 \\ \frac{V_2^2}{V_1} + \frac{V_1^2}{2Fr^2} \end{pmatrix}$. Firstly, we concentrate only on the G_{HR} part which gives the classical Shallow Water equations and apply the (first-order) hydrostatic reconstruction. As the method is fully described in the literature (see e.g. [6, 2, 10]) and is not specific to our case, we just set we construct V_i^{n+1} for the shallow water part thanks to this way. The last step concerns only hU:

$$(hU)_i^{n+1} = (hU)_i^{n+1} - \frac{\Delta t}{\Delta x} \left[F(V_i^n, V_{i+1}^n) - F(V_{i-1}^n, V_i^n) \right] - \Delta t \bar{\delta} \frac{((u_e)_i^{n+1})^2 \alpha_2 \varphi'(0)}{w_i^{n+1}}$$

where F is obtained from $G(V) = \bar{\delta} u_e^2 \delta_1 (1 - \frac{1}{H}) - \frac{(\bar{\delta} u_e \delta_1)^2}{V_1}$.

To conclude the presentation of the used code, we precise that we take an uniformly discretized space $[a, b]$ where the cell length Δx is got thanks to J the number of points for the space mesh. As regards the time discretization, we use an adaptive cell length Δt calculated at each time step with a CFL condition $\Delta t = \frac{n_{CFL} \Delta x}{c}$. The speed propagation c is estimated with the four eigenvalues of the block diagonal matrix (5.1).

Remark 5.1. *As said previously, the velocity profile is fixed in the computations. The choice (linear or parabolic) is indicated in the captions of the figures.*

Remark 5.2. *The quantities are made non dimensional with say meters, seconds... so that* $g = 9.81$. *Examples, except those with transcritical phenomena, are subcritical* ($Fr < 1$).

5.2 Shallow water system without friction vs ESW system

As we saw before, theoretically the ESW model includes the shallow water model if the effective Reynolds number εRe is infinite. So the first numerical verification is to check the concordance between the two models. To illustrate this point, we present three cases: a subcritical flow over a Gaussian bump, and two transcritical flows, one without shock and one with shock [17]. Notice that analytic solutions exist for these three academic examples, see [12]. However, we choose here to discretize the shallow water model with the same finite volume scheme as the ESW system.

5.2.1 Subcritical flow

In this case, the ground is a Gaussian bump $f_b(x) = \frac{1}{50} \exp(-\frac{(x-0.5)^2}{2(0.05)^2})$.

Initial conditions are taken equal to

$$V_0 = \begin{pmatrix} h \\ U \\ \delta_1 \\ u_e \end{pmatrix} = \begin{pmatrix} 1 - f_b \\ 1 \\ 0.01 \\ 1 \end{pmatrix}$$

and for the boundary conditions

$$\begin{cases} \text{upstream: } \begin{pmatrix} h \\ U \\ \delta_1 \\ u_e \end{pmatrix} = V_0 \\ \text{downstream: free.} \end{cases}$$

On figure 6, we plotted the results for the shallow water model without friction and for the ESW system. The simulation for $\varepsilon Re = 10^8$ answers our expectation since the shallow water curves are the same as those of ESW for the heights and velocities. Therefore we can observe that for a lower Reynolds number, $\varepsilon Re = 10^4$, the shallow water velocity is higher than the ESW velocity. Since a lower Reynolds number expresses a larger viscosity, hence higher friction, this phenomenon is expected: the flow slows down. We complement the figures for the two Reynolds number by simulations of the displacement thickness δ_1.

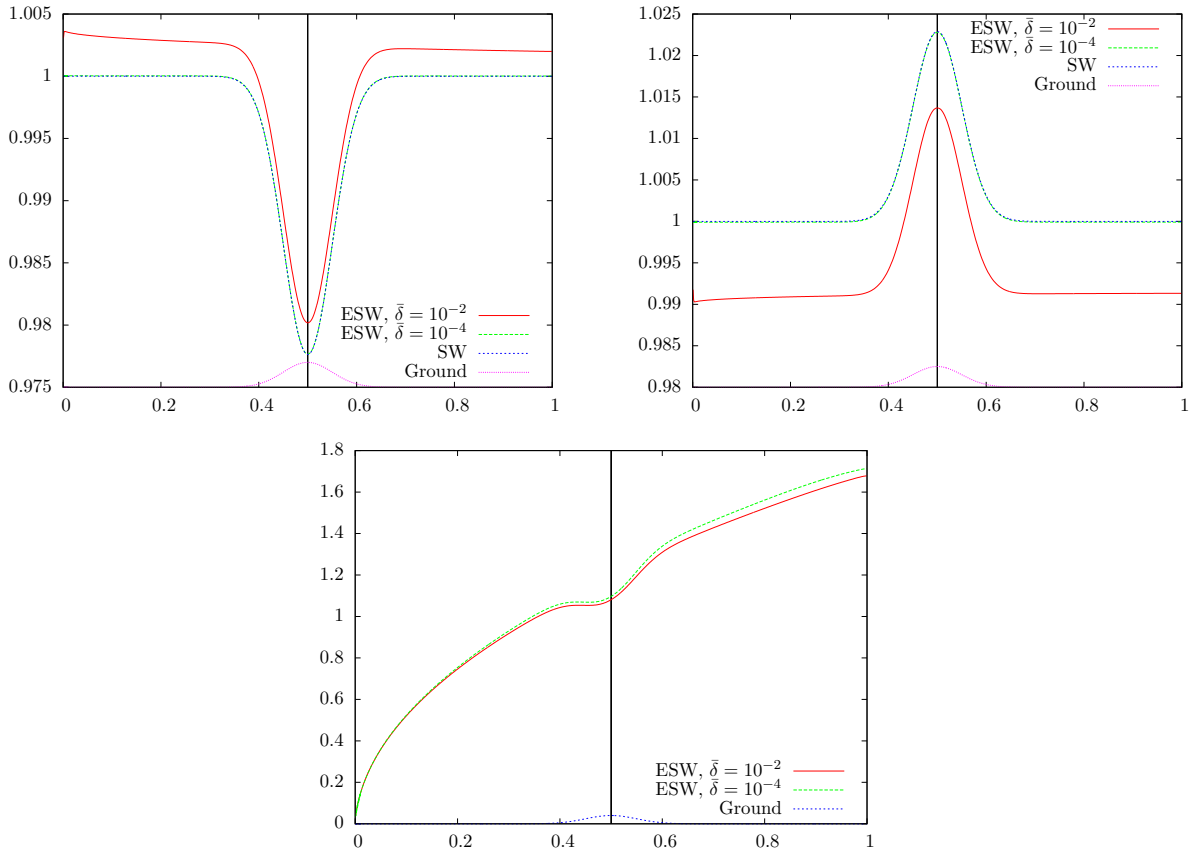

Figure 6: Subcritical flows–Heights in the top left corner , velocities in the top right corner for ESW model and SW without friction, displacement thickness at the bottom–Simulations with $T = 3$, $J = 800$, $f_b(x) = \frac{1}{50}\exp(-\frac{(x-0.5)^2}{2(0.05)^2})$, linear profile. The SW curve and the ESW one for $\bar{\delta} = 10^{-4}$ are superposed, but distinguish themselves for $\bar{\delta} = 10^{-2}$.

5.2.2 Transcritical flows

For the two transcritical flows, the studied topography is the one studied in [17]:

$$f_b(x) = \left[0.2 - 0.05(x-10)^2\right] \mathbb{1}_{[8,12]}(x) \qquad x \in [0, 25].$$

Usually the initial conditions are a lake at rest. Due to the naive computation of the ESW, $u_e = 0$ and $\delta_1 = 0$ is not allowed. For initial conditions of h and U we take the usual ones as in [17], and we choose small values for u_e and δ_1. In each case (see figure 7 for the transcritical without shock case and figure 8 for the transcritical with shock one), the simulations give a behavior of the surface η and the velocity U not disturbed on the bump for the two Reynolds number in comparison with the Shallow Water curves but some changes on the flat parts of the ground appear for the smallest Reynolds number presented. We find also this result for the displacement thickness δ_1.

- **Transcritical flow without shock**

  The transcritical flow without shock (see figure 7) illustrates a subcritical upstream flow which becomes supercritical at the top of the bump. The initial conditions are :

$$\begin{pmatrix} h \\ U \\ \delta_1 \\ u_e \end{pmatrix} = \begin{pmatrix} 0.66 - f_b \\ 0 \\ 0.01 \\ 0.01 \end{pmatrix}.$$

For the boundary conditions, we choose:

$$\begin{cases} \text{upstream: } hU = 1.53,\ u_e = \frac{1.53}{h},\ u_e\delta_1 = (0.01)^2, \\ \text{downstream: } h = 0.66 \text{ while the flow is subcritical.} \end{cases}$$

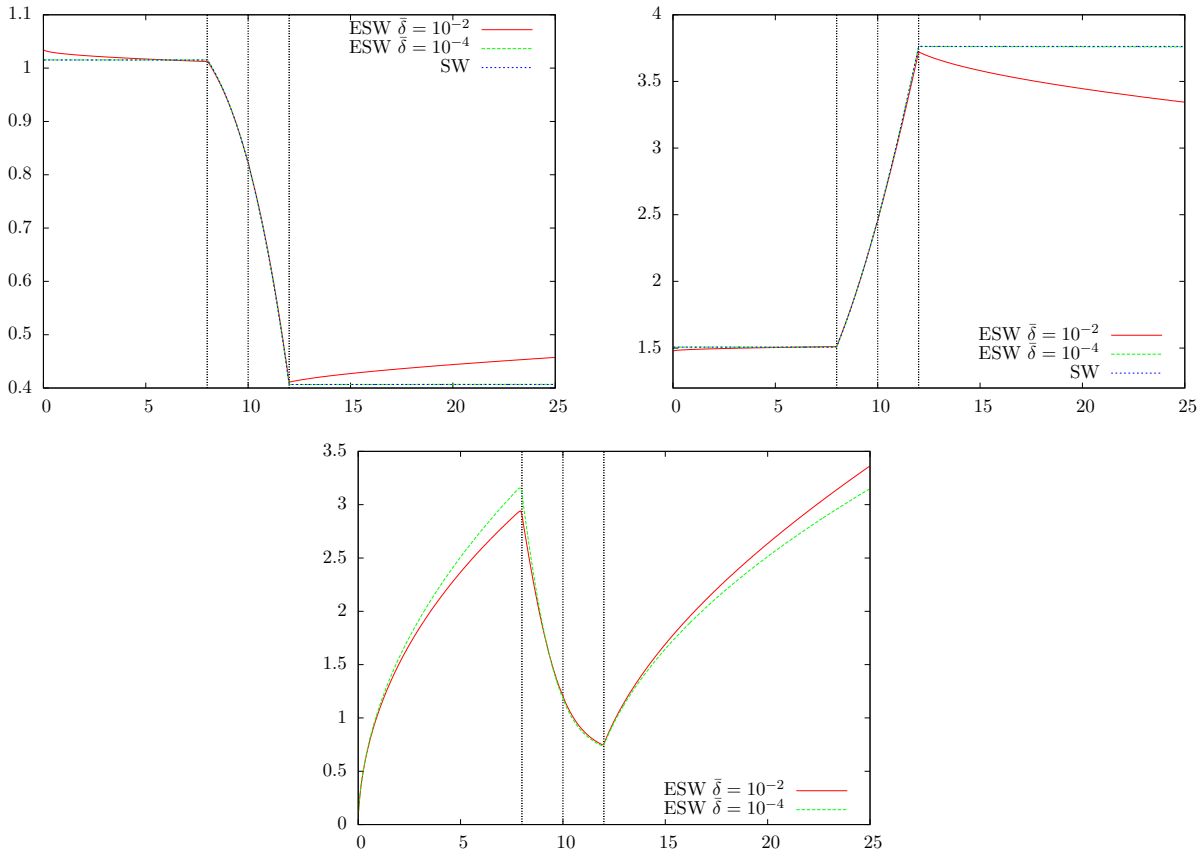

Figure 7: Transcritical without shock flows–Surface $\eta = h + f_b$ in the top left corner , velocities in the top right corner for ESW model and SW without friction, displacement thickness at the bottom– Simulations with $J = 800$, $T = 150$, linear profile and the vertical dashed draws represent the key points of the ground. ESW curve for $\bar{\delta} = 10^{-4}$ and the SW one are superposed. The ESW one for $\bar{\delta} = 10^{-2}$ distinguishes itself from the others on the flat areas of the topography, which can be explained by the behavior of the displacement thickness.

- **Transcritical flow with shock.** In this part, we keep the same parabolic bump but we change the flow conditions so that the flow becomes supercritical on the top of the bump and then fluvial again after a hydraulic jump. Compared to computations using the Shallow Water model, we recover the hydraulic jump at a position which is consistent with the classical SW model, but slightly depends on the value of $\bar{\delta}$, see Figure 8, top. However, the stabilization of δ_1 after the shock is not ensured for "large" values of $\bar{\delta}$, see Figure 8, bottom. Actually, we observe some time instability after the hydraulic jump for these values of $\bar{\delta}$, see Figure 9. This can question both the model and the numerical resolution. Indeed concerning numerics, we are faced for δ_1 with an equation where the transport operator contains a discontinuous velocity field, which can induce stability problems. On the other hand, we also reach the limits of the model itself since most likely some recirculation phenomena occur after the jump, and this is not accounted for in this model.

Initial conditions:

$$\begin{pmatrix} h \\ U \\ \delta_1 \\ u_e \end{pmatrix} = \begin{pmatrix} 0.33 - f_b \\ 0 \\ 0.01 \\ 0.01 \end{pmatrix}.$$

For the boundary conditions, we choose:

$$\begin{cases} \text{upstream: } hU = 0.18,\ u_e = \frac{0.18}{h},\ u_e\delta_1 = (0.01)^2, \\ \text{downstream: } h = 0.33. \end{cases}$$

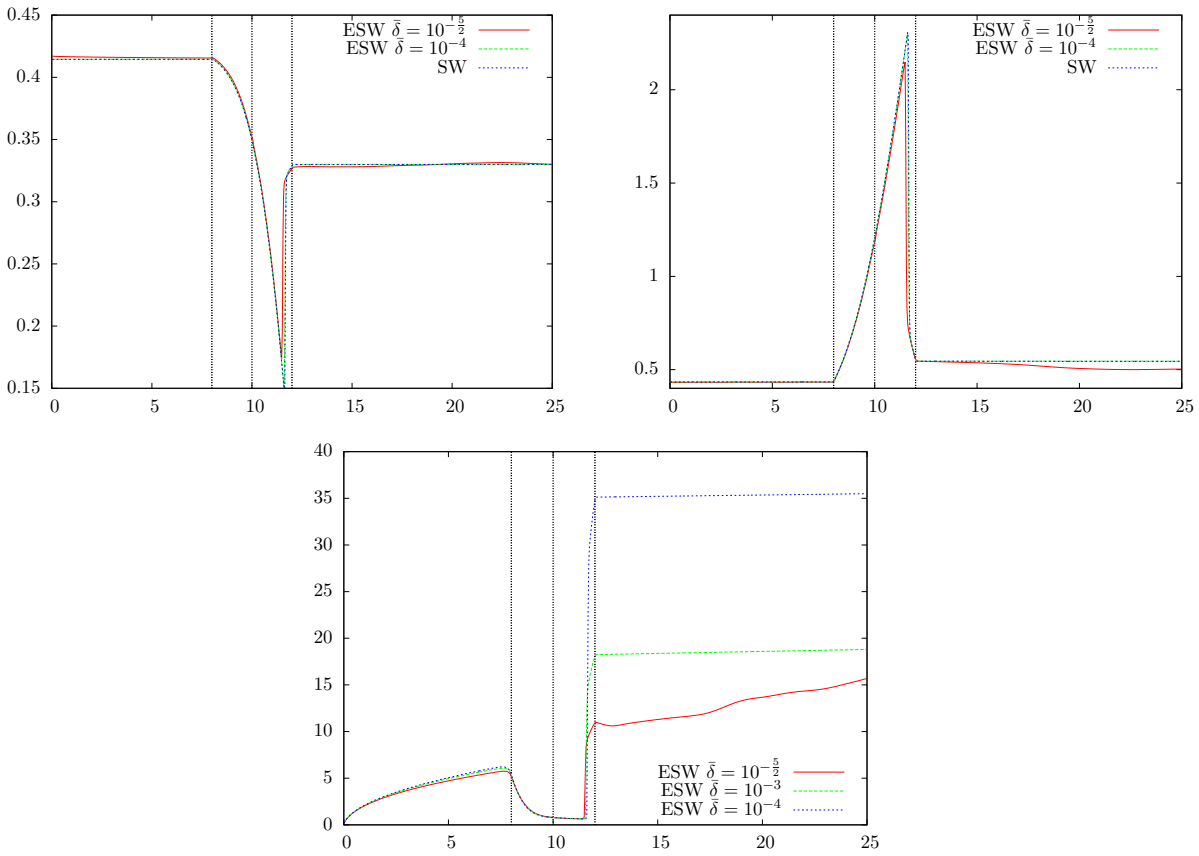

Figure 8: Surface $\eta = h + f_b$ (top left), velocity U (top right) and displacement thickness (bottom) for transcritical flow with shock for the Shallow Water model (SW) and two values of $\bar{\delta}$ for the ESW model –$J = 800$, $T = 590$, linear profile. Differences between the SW model and the ESW model are especially seen on the flat parts of the ground, even if there is also a difference on the amplitude at the end of the bump.

5.3 Stationary solution on a flat ground

In part 4.3, we established, on a flat ground, a stationary solution for our system linearized with respect to $\bar{\delta}$:

$$\begin{cases} \delta_1^0 = \sqrt{\frac{2\alpha_2 H}{u_e}\varphi'(0)}\sqrt{x}, \quad u_e = u_e^0 + \bar{\delta}\frac{U^0}{h^0}\frac{1}{1-Fr_0^2}\delta_1^0 \\ h = h^0 + \bar{\delta}\frac{Fr_0^2}{Fr_0^2-1}\delta_1^0, \quad U = U^0 + \bar{\delta}\frac{U^0}{h^0}\frac{Fr_0^2}{1-Fr_0^2}\delta_1^0, \end{cases}$$

where h^0, U^0, u_e^0 are constants and $u_e^0 = U^0$. To be satisfying, the numerical scheme presented in this section must be consistent with it. On the figure 10, we can observe the analytic linearized solution and the computed

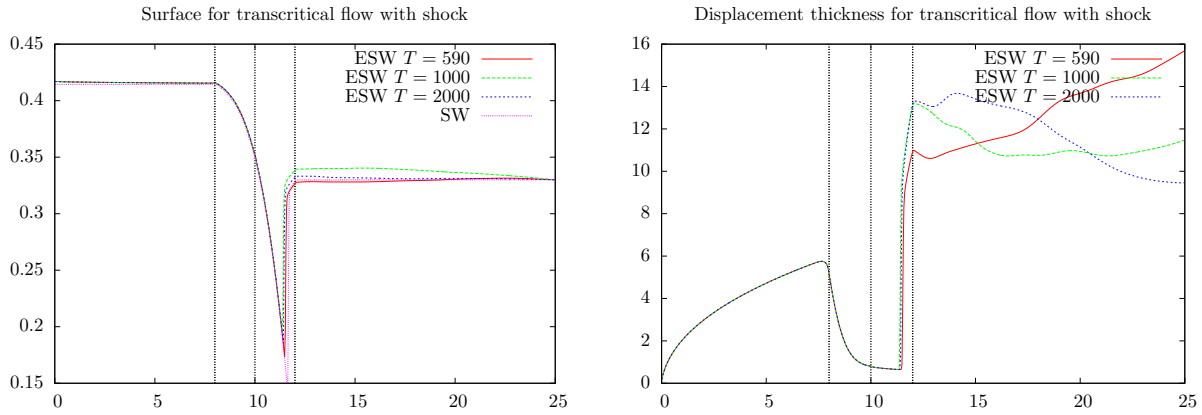
Surface for transcritical flow with shock
ESW $T = 590$
ESW $T = 1000$
ESW $T = 2000$
SW
Displacement thickness for transcritical flow with shock
ESW $T = 590$
ESW $T = 1000$
ESW $T = 2000$

Figure 9: Time evolution of surface $\eta = h + f_b$ (left) and displacement thickness (right) for transcritical flow with shock for the Shallow Water model (SW) with $\bar{\delta} = 10^{-5/2}$. Instability is clearly evidenced after the jump position.

solutions for two values of $\bar{\delta}$. The entrance boundary condition is not sophisticated enough and so there is an initial difference which appears. Nevertheless, we can observe a very good similitude for the value $\bar{\delta} = 10^{-4}$. On the other way, for $\bar{\delta} = 10^{-2}$ the computed solution gets away from the analytic one with especially a different behaviour in space. This observation is consistent with the steady state for the von Kármán equation presented in the section 4.2.

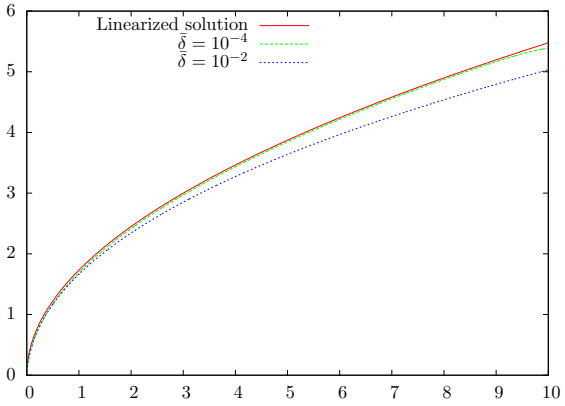

Figure 10: Analytic displacement thickness for two values of $\bar{\delta}$, $J = 2000$, $T = 30$, flat ground, linear profile. The theoretical solution does not depend of $\bar{\delta}$ and so all the solutions can be plotted on the same figure. For $\bar{\delta} = 10^{-2}$ and for a longer space, the computed solution does not follow the Blasius solution but slows down.

5.4 ESW over a Gaussian bump

The concordance observed between the shallow water model without friction and the ESW system, we will now observe more precisely the behavior of the displacement thickness as well of the friction term in response to a parametrized bump.

For the following simulations, we choose for the ground a Gaussian profile:

$$f_b(x) = A \exp(-\frac{(x-m)^2}{2\sigma^2}).$$

The initial conditions, by default, are on the form $V_0 = \begin{pmatrix} h \\ U \\ \delta_1 \\ u_e \end{pmatrix} = \begin{pmatrix} 1 - f_b \\ 1 \\ 0.01 \\ 1 \end{pmatrix}$. The considered flow is subcritical, and as regards the boundary conditions we consider

$$\begin{cases} \text{upstream: } \begin{pmatrix} h \\ U \\ \delta_1 \\ u_e \end{pmatrix} = V_0 \\ \text{downstream: free} \end{cases} .$$

The following illustrations place themselves in case where the displacement thickness is developing. Even if a Gaussian bump locates in the middle of the simulation, the behavior for the displacement thickness stays the Blasius solution 4.3 which will be more or less disturbed by the bump as seen in the figure 11. This global growing shape may interfere with the local observations of the effects (especially for the friction term τ because of large first values). To rectify this, we will present as well some figures rescaled by the Blasius solution. Due to the monoticity of the rescaling functions, the local extrema observed will be moved downstream in comparison with the displacement thickness or friction term without the rescaling.

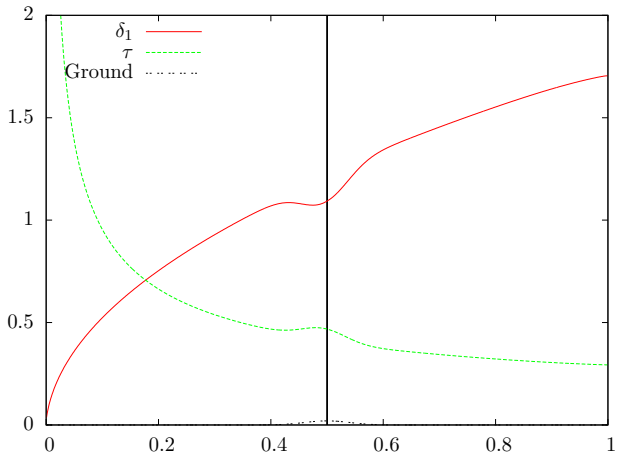

Figure 11: Displacement thickness δ_1 and friction term τ over a Gaussian bump– $f_b(x) = \frac{1}{50}\exp(\frac{-(x-0.5)^2}{2(0.04)^2})$, $T = 3$, $J = 800$, $\bar{\delta} = 10^{-3}$, linear profile. The displacement thickness thins down under the bump influence in spite of the global Blasius shape. Consequently the friction term $\tau = \frac{u_e \alpha_2 \varphi'(0)}{\delta_1}$ presents a growing near the bump.

Remark 5.3. *The plotted bump in the following figures is just an indicative one. The width is respected but not the amplitude nor the ordinate.*

5.4.1 Improved friction term

The shallow water theory already allows to treat a viscosity effect thanks to added terms in the momentum equation (see 1.3). However they do not fit with the expectations, that is to say a friction more significant just before the top of the bump as in [22]. In this part, we will observe more in details the local extrema observed in the previous figure 11. Then we will compare with the laminar friction in the SW model.

The figure 12 is only a zoom of figure 11 where the extrema are evidenced. We can observe that the local minimum for the displacement thickness is located before the top of the bump. Even if the abscissa of the maximum of τ is moved on the right (due to the growing of u_e which compensate the decrease of $1/\delta_1$), the local maximum is reached upstream the top of the bump.

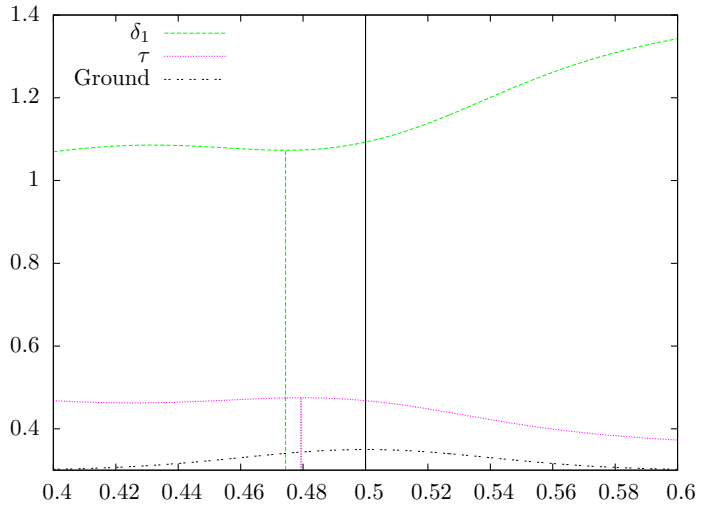

Figure 12: Displacement thickness and friction term over a bump– $f_b(x) = \frac{1}{50}\exp(-\frac{(x-0.5)^2}{2(0.04)^2})$, $\bar{\delta} = 10^{-3}$, $T = 3$, $J = 800$, linear profile. Maximum of friction term is in advance from the top of the bump.

The comparison between SW with friction and ESW models brings out an issue as the level of friction are different. The Poiseuille-shallow water (see section 1.3) gives a friction term in $\bar{\delta}^2$ whereas the ESW one is in $\bar{\delta}$. The difference does not allow to plot the friction terms in the same window. Also, in place of $\frac{3\bar{\delta}^2 U}{h}$, we choose to take the laminar friction term for the shallow water model on the form $C_l\frac{U}{h}$ where the coefficient C_l is adapted by hand. We fix $C_l = 0.00068$ to fit the velocities between SW and ESW simulations when $\bar{\delta} = 0.001$ (recall that ESW friction is $\bar{\delta}\tau$). The consequence on the friction terms is presented in the figure 13. The laminar SW term has its maximum at the top of the bump which is not physically expected. Due to the only dependence in the velocity and the height (the two unknowns of the shallow water equations), other patterns would have the same defect.

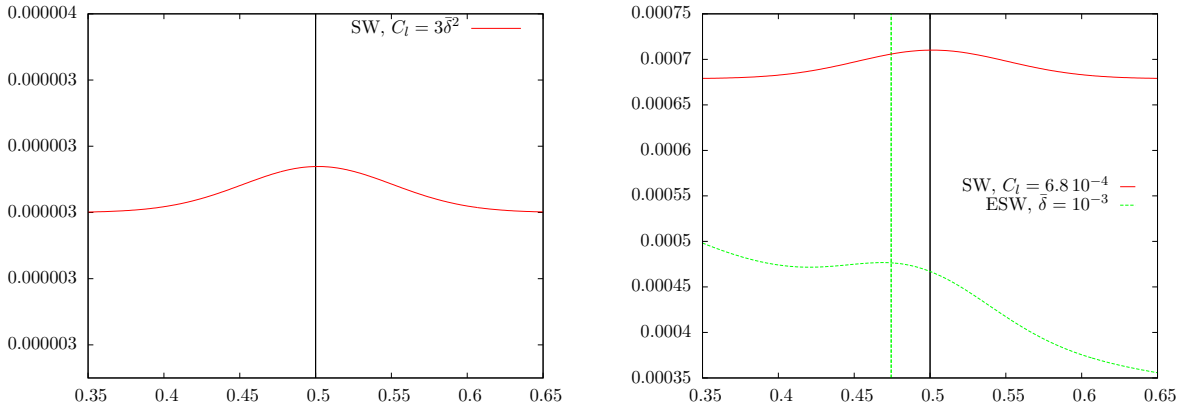

Figure 13: Friction terms: on the left we have the Poiseuille-shallow water friction and on the right a comparison between a laminar shallow water friction scaled by hand and the ESW friction– $x \in [0.35, 0.65]$; $f_b(x) = \frac{1}{50}\exp(-\frac{(x-0.5)^2}{2(0.05)^2})$; $J = 800$; $T = 3$; $\bar{\delta} = 10^{-3}$; linear profile.

5.4.2 Influence of $\bar{\delta}$

The parameter $\bar{\delta} = \frac{1}{\sqrt{\varepsilon Re_h}}$ controls the thickness of the viscous layer. It is the key point of the ESW model. Also, we will observe here the influence of its value for the shape of the displacement thickness δ_1 and the friction τ. The physical values are $\bar{\delta}\delta_1$ and $\bar{\delta}\tau$, but to compare them we plot only δ_1 and τ. On the flat ground before the bump, the displacement thickness is nearly conserved as we can see in the figure 14, excepted for $\bar{\delta} = 0.1$ which is explained by the limitation of the scheme. Around the bump a net difference appears even if it is more noticeable on the right of the bump. Anyway δ_1 gets down with the growing of $\bar{\delta}$ but conserves its shape and the local minimum abscissa for δ_1 is not influenced by $\bar{\delta}$. This statement holds as far as $\bar{\delta}$ is not big since $\bar{\delta} = 0.1$ begins to show a significantly disruption from the beginning. Taking a huger value for $\bar{\delta}$ leads to great instabilities and the scheme not hold.

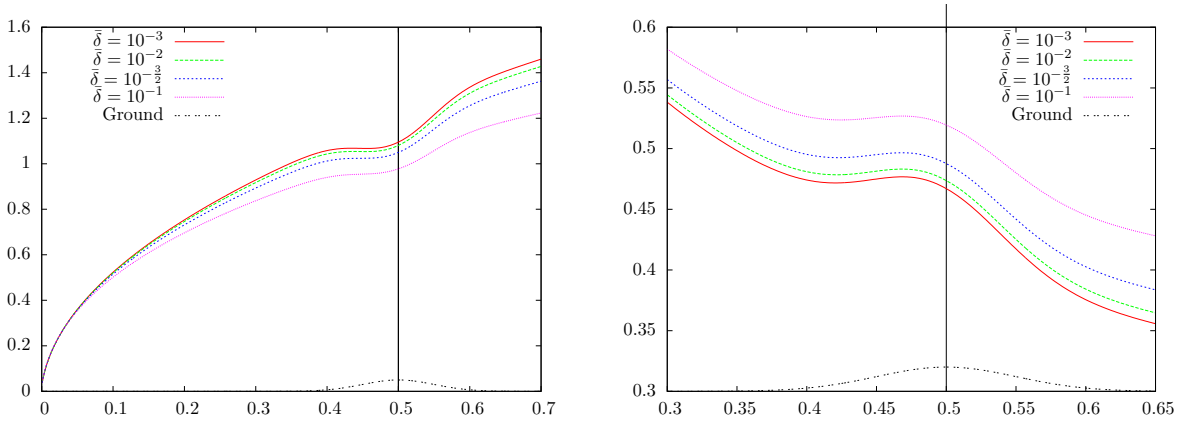

Figure 14: Influence of $\bar{\delta}$ on displacement thickness δ_1 (left) and friction term τ (right) – $f_b(x) = \frac{1}{50}\exp(-\frac{(x-0.5)^2}{2(0.05)^2})$, $J = 800$, $T = 3$, linear profile. The local extrema are not displaced by the variation of $\bar{\delta}$, except for $\bar{\delta} = 0.1$.

5.4.3 Influence of the bump shape ($Fr < 1$)

Bump amplitude. Not very surprisingly, the bump amplitude has a direct influence on the amplitude of variation of δ_1 and τ. On the one hand, as it is seen in figure 15, the smaller the amplitude, the closer δ_1 is to the Blasius solution. On the other hand, it can be observed that the solution departs from the Blasius one after the bump when the amplitude increases. This phenomenon becomes important for large values of the amplitude (see Figure 17), and might be bound with the boundary layer separation when the downstream slope of the bump becomes too high (see for instance [24]). We can not, with the chosen profiles here compute boundary layer separation.

Remark 5.4. *The figure 15 illustrates the limitation of the local extrema observation due to the square root shape (or inverse of a square root for the friction term τ). When the amplitude tends to zero, an inflection point stays but it is difficult to locate the precise abscissa. Even if the rescaled outline moves the abscissa of the extrema to the right, the figure 16 allows to observe quantitatively the amplitude influence on δ_1 and τ.*

The variation of the bump amplitude brings out another property for the displacement thickness. As far the amplitude is sufficient, the displacement thickness catches up always the same curve around the bump and that, for different initial values. In all the previous examples, δ_1 was initialized by $\delta_1 = 0.01$. This choice of a small value for δ_1 was intended to observe the development of the viscous layer. Starting with a constant value not morally equal to zero is interpreted as an established viscous flow in entry. In the figure 18, this initial value varies with a given bump. Even if the Blasius behavior described by the equation 4.3 begins at different values, around the bump the four curves are gathered. So there is an independence of the solution around the bump

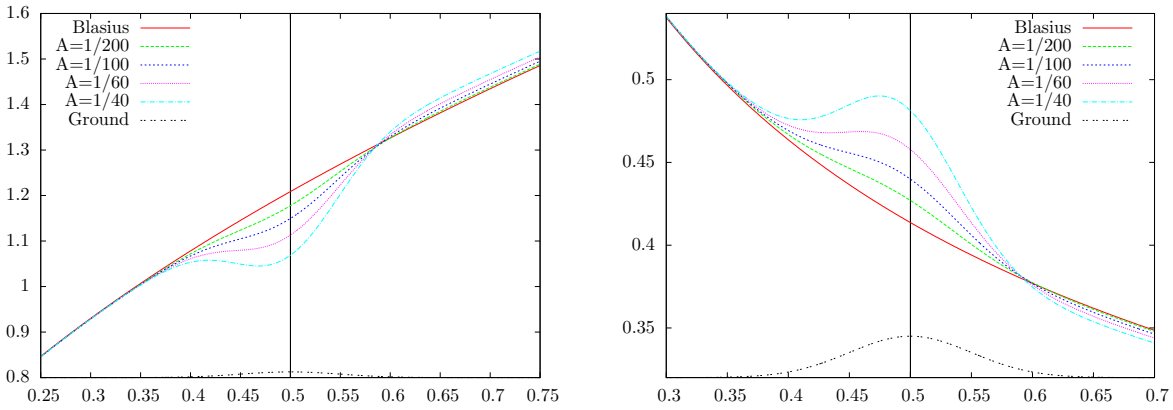

Figure 15: Bump amplitude: displacement thickness δ_1 (left) and zoom on the friction term τ (right) – $f_b(x) = A\exp(\frac{-(x-0.5)^2}{2(0.05)^2})$, $T = 3$, $J = 800$, $\bar{\delta} = 10^{-3}$, linear profile.

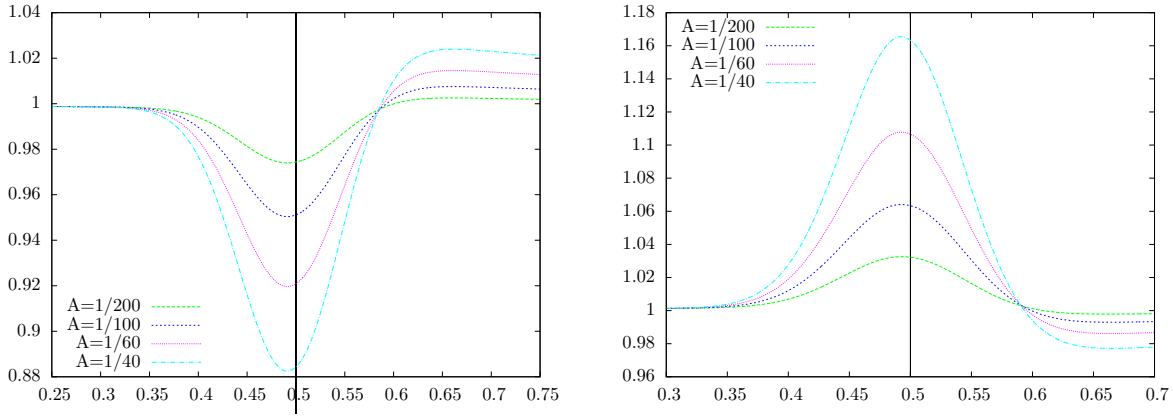

Figure 16: Bump amplitude: displacement thickness δ_1 (left) and zoom on the friction term τ (right) with a rescaling by the Blasius solution– $f_b(x) = A\exp(\frac{-(x-0.5)^2}{2(0.05)^2})$, $T = 3$, $J = 800$, $\bar{\delta} = 10^{-3}$, linear profile.

with respect to the initial value for the displacement thickness, even if the phenomenon can not be observed for every entrance and is limited by the bump amplitude choice.

Bump width. The bump width is quantified by the standard deviation σ in the Gaussian profile. Increasing the width of the bump increases as well the extent of the response of both δ_1 and τ, see figures 19 and 20. The amplitude is also slightly decreased. But the most interesting phenomenon is that the local maximum of the friction moves upstream from the top of the bump. Nevertheless, since the response of the displacement thickness spreads with the bump width, a too much broad bump leads only to an inflection point. Rescaling functions in Figures 19 and 20 are more appropriated to observe the phenomenon.

5.4.4 Velocity profile

As we have seen in the section 2.3, a key role for the ESW model is played by the velocity profile φ. Several choices can be made for a better answer when the viscous velocity significantly varies. A refined way would be an adjustable profile to react faster over a bump (see [24]). Once again, in this paper we will restrict to the easiest computations: the linear and parabolic profiles. Table 1 references the resultant values for α_2, H and $\varphi'(0)$ the three parameters encountered in the system. In the following figures 21 and 22, we plotted the displacement thickness δ_1 and the friction term τ for these two profiles. The parabolic profile presents an advanced reaction, in relation to the top of the bump, compared to the linear profile. The phenomenon is clearer for the displacement

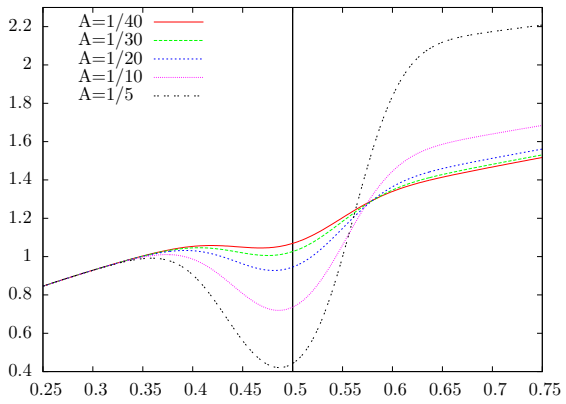

Figure 17: Bump amplitude: displacement thickness δ_1–$f_b(x) = A\exp(\frac{-(x-0.5)^2}{2(0.05)^2})$; $J = 800$; $T = 3$; $\bar{\delta} = 10^{-3}$, linear profile. High bump leads to a disruption downstream the bump of the Blasius behavior of δ_1.

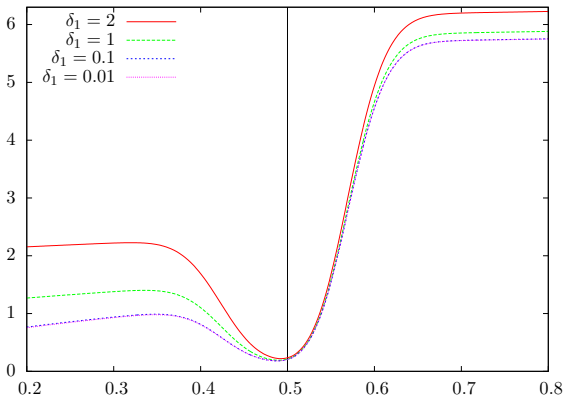

Figure 18: Influence of the initial data for the displacement thickness δ_1 – $f_b(x) = \frac{1}{3}\exp(\frac{-(x-0.5)^2}{2(0.05)^2})$; $J = 800$; $\bar{\delta} = 10^{-3}$; $T = 3$, linear profile.

thickness than the friction term. This difference is explained by the expression of $\tau = \frac{u_e \alpha_2 \varphi'(0)}{\delta_1}$. $\varphi'(0)$ and α_2 are constant for these profiles but u_e, which is growing in this zone, plays a determinant role in the position of the local maximum.

6 Conclusion

This paper concerns a shallow water model with an improved description in the long wave and large Reynolds limit of the flow and the parietal friction. This model consists of a system of four equations (3.8), (3.9), (3.10) and (3.12): two are similar to shallow water system (mass and momentum conservation) with a supplementary term describing momentum flux, one ideal fluid equation and the von Kármán equation to describe the viscous layer development. The boundary layer acts as a new topography for the model (Eq. 3.11). This model is an example of "Interactive Boundary Layer" or "Viscous Inviscid Interaction". The flux in the momentum equation (3.9) contains not only the hydrostatic pressure term $h^2/(2Fr)$ but an additional correction term of the same order of magnitude as the friction. The friction term is no longer a combination of velocity and depth (as in usual laws such as Darcy or Manning) but the result of a viscous boundary layer like approach (Eq. (3.12)).

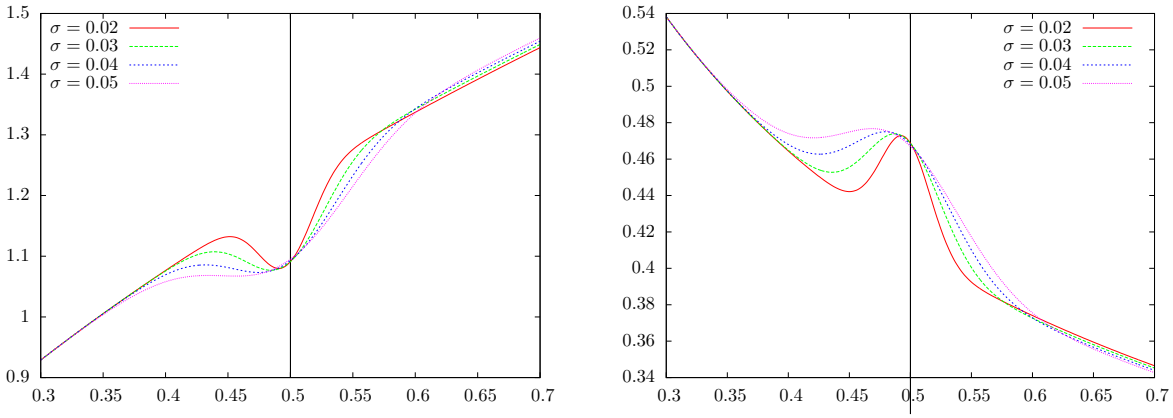

Figure 19: Influence of the bump width over the displacement thickness δ_1 (left) and friction τ (right) – $f_b(x) = \frac{1}{50}\exp(-\frac{(x-0.5)^2}{2\sigma^2})$; $J = 800$; $T = 3$; $\bar{\delta} = 10^{-3}$, linear profile. The abscissa of the local extrema depends on the width of the bump.

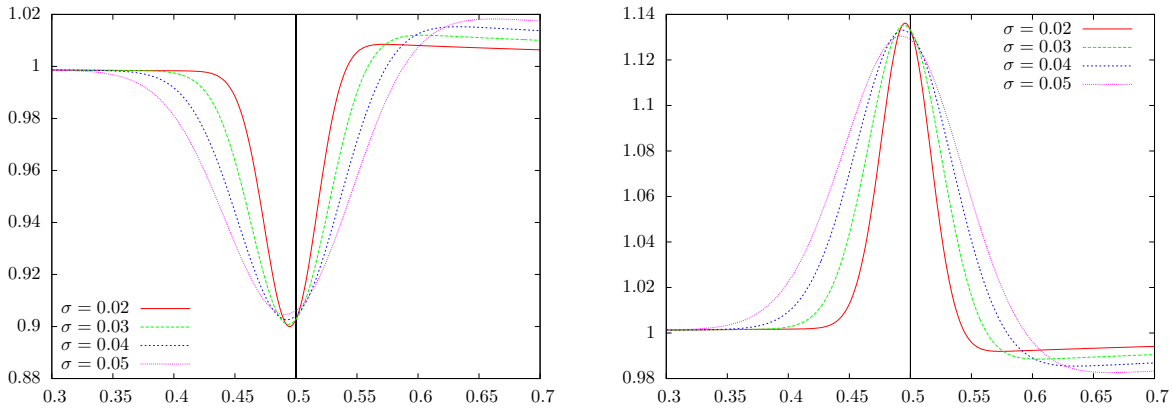

Figure 20: Influence of the bump width with rescaling by the Blasius solutions: displacement thickness on the left and friction term on the right – $f_b(x) = \frac{1}{50}\exp(-\frac{(x-0.5)^2}{2\sigma^2})$; $J = 800$; $T = 3$; $\bar{\delta} = 10^{-3}$, linear profile. The abscissa of the local extrema depends on the width of the bump.

As it is, it actually depends on the topography, as evidenced by the examples provided in the last part of the work. In particular its maximum is reached before the summit of a bump. This effect is limited here, and it is a limitation of this work, because the velocity profiles used lead to constant shape and friction coefficients. As a consequence, possible boundary layer separation with recirculation downstream of the bump cannot be observed. Imposing a family of adjustable profiles will be the next step, this should enhance the effects of topography. Results from [5, 22, 23] in case of flows in pipes, and preliminary comparisons with multilayer shallow water [3] make us confident. The main drawback of this model is the viscous layer/ideal fluid decomposition, which forbids the viscous layer to fill all the water depth far downstream of the bump. Extra modelling in this direction and more examples have now to be worked out and tested, an effort has to be done as well to improve the numerical method. Finally, even thoug this approach is restricted here to laminar flows, the ideas developed here can be extended with little modifications to mean turbulent profiles.

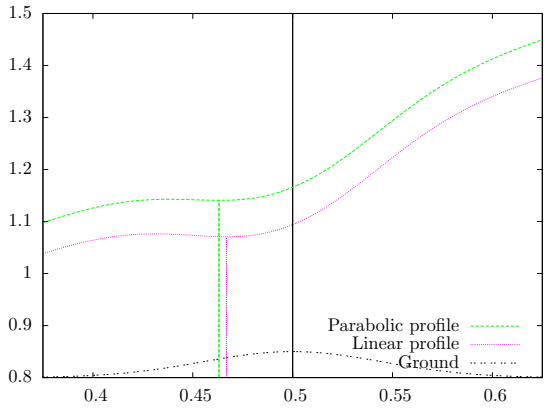

Figure 21: Displacement thickness for two different profiles φ– $f_b(x) = \frac{1}{50}\exp(-\frac{(x-0.5)^2}{2(0.045)^2})$; $J = 800$; $T = 3$; $\bar{\delta} = 10^{-3}$. The curves shape are similar but the parabolic profile is advanced in regard to the linear one.

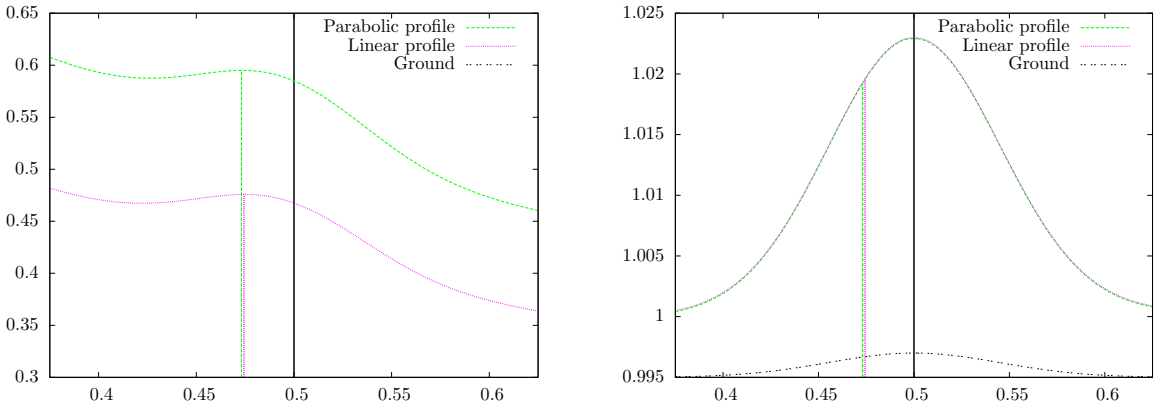

Figure 22: Friction terms for two different profiles φ on the left and the velocity u_e on the right– $x \in [0.375, 0.625]$; $f_b(x) = \frac{1}{50}\exp(-\frac{(x-0.5)^2}{2(0.05)^2})$; $J = 800$; $T = 3$; $\bar{\delta} = 10^{-3}$. The variations of u_e explain that local maximums for the friction get closer in abscissa (these ones are figured on the plot) in comparison with the local minimums for the displacement thickness seen in the figure 21.

References

[1] F. Alcrudo & E. Gil. *The Malpasset dam break case study.* Proceedings of the 4^{th} Concerted Action on Dambreak Modelling Workshop, pages 95-109, Zaragoza, Spain, 1999.

[2] E. Audusse, F. Bouchut, M.-O. Bristeau, R. Klein & B. Perthame, *A fast and stable well-balanced scheme with hydrostatic reconstruction for shallow water flows*, SIAM Journal on Scientific Computing, **25** (2004), n^o 6, 2050-2062

[3] E. Audusse, M.-O. Bristeau, B. Perthame & J. Sainte-Marie. *A multilayer Saint-Venant system with mass exchanges for shallow water flows. Derivation and numerical validation*, ESAIM: M2AN, **45** (2011), 169-200

[4] A.J.C Barré de Saint-Venant. *Théorie du mouvement non-permanent des eaux, avec application aux crues des rivières et à l'introduction des marées dans leur lit*, C. R. Acad. Sci., **73** (1871), 147-154

[5] E. Berger, M. Deverge, A. Hirschberg, P.-Y. Lagrée & C. Vilain, *Characterization of the pressure drop in a 2D symmetrical pipe: some asymptotical,, numerical and experimental comparisons*, ZAMM: Z. Angew. Math. Mech. **85** (2005), n^o 2, 141-146

[6] F. Bouchut, **Nonlinear Stability of Finite Volume Methods for Hyperbolic Conservation Laws and Well-Balanced Schemes for Sources**. Bierkhäuser, 2004.

[7] J. Burguete, & P. García-Navarro, *Implicit schemes with large time step for non-linear equations: application to river flow hydraulics*, International Journal for Numerical Methods in Fluids, **46** (2004), n^o 6, 607-636

[8] V. Caleffi, A. Valiani & A. Zanni. *Finite volume method for simulating extreme flood events in natural channels.* Journal of Hydraulic Research, 41(2):167-177, 2003.

[9] V.T. Chow. **Open-channel hydraulics**. McGraw-Hill, New-York, USA, 1959.

[10] O. Delestre, S. Cordier, F. Darboux & F. James. *A limitation of the hydrostatic reconstruction technique for shallow water equations.* C. R. Acad. Sci. Paris, Sér. I 350, pp 677-681, 2012.

[11] O. Delestre, S. Cordier, F. James & F. Darboux. *Simulation of rain-water overland-flow.* In E. Tadmor, J.-G. Liu and A. Tzavaras, editors, Proceedings of the 12^{th} International Conference on Hyperbolic Problems, volume 67 of Proceedings of Symposia in Applied Mathematics, pages 537-546, University of Maryland, College Park (USA), 2009. Amer. Math. Soc.

[12] O. Delestre, C. Lucas, P.-A. Ksinant, F. Darboux, Ch. Laguerre, T.-N.-T. Vo, F. James & S. Cordier, *SWASHES: a compilation of shallow water analytic solutions for hydraulic and environmental studies*, Int. J. Numer. Meth. Fluids (2012)

[13] M. Esteves, X. Faucher, S. Galle & M. Vauclin. *Overland flow and infiltration modelling for small plots during unsteady rain: numerical results versus observed values.* Journal of Hydrology, 228(3-4): 265-282, 2000.

[14] S.L. Gavrilyuk & G.L. Richard. *A new model of roll waves: comparison with Brock's experiments.* J. Fluid Mech., volume 698, pp374-405, 2012.

[15] J.-F. Gerbeau & B. Perthame, *Derivation of viscous Saint-Venant system for laminar shallow water; numerical validation*, Discrete and Continuous Dynamical Systems: Series B **1** (2001), n^o 1, 89-102

[16] D.L. George. *Finite volume methods and adaptive refinement for tsunami propagation and inundation.* PhD thesis, University of Washington, USA, 2006.

[17] N. Goutal & F. Maurel. *Proceedings of the 2^{nd} workshop on dam-break wave simulation.* Technical Report HE-43/97/016/B, Electricité de France, Direction des études et recherches, 1997.

[18] R.S. Govindaraju *Modeling overland flow contamination by chemicals mixed in shallow soil horizons under variable source area hydrology*, Water Resources Research, **32** (1996), n^o 3, 753-758

[19] A. J. Hogg & D. Pritchard. *The effects of hydraulic resistance on dam-break and other shallow inertial flows.* J. Fluid Mech. volume 501, pp179-212, 2004.

[20] S. Kalliadasis, C. Ruyer-Quill, B. Scheid & M. G. Velarde. *Falling Liquid Films.* Applied Mathematical Sciences, volume 176. Springer London, 2012.

[21] D.-H. Kim, Y.-S. Cho & Y.-K. Yi. *Propagation and run-up of nearshore tsunamis with HLLC approximate Riemann solver.* Ocean Engineering, 34(8-9): 1164-1173, 2007.

[22] P.-Y. Lagrée & S. Lorthois. *The RNS/Prandtl equations and their link with other asymptotic descriptions. Applications to the computation of the maximum value of the Wall Shear Stress in a pipe.* Int. J. Eng Sci., volume 43/3-4 pp352-378, 2005.

[23] P.-Y. Lagrée, A. Van Hirtum & X. Pelorson (2007) *Asymmetrical effects in a 2D stenosis*, European Journal of Mechanics B/Fluids, **26**, Issue 1, January February 2007, 83-92

[24] P.-Y. Lagrée. *Asymptotic Methods in Fluid Mechanics: Survey and Recent Advances, CISM Courses and lectures, volume 523.* Springer-Verlag, Wien New York, 2010.

[25] M.-H. Le, S. Cordier, C. Lucas, O. Cerdan, *A faster numerical scheme for a coupled system modeling soil erosion and sediment transport*, Water Resources Research, **51** (2015), 987-1005

[26] S. Popinet. *Quadtree-adaptative tsunami modelling*. Ocean Dynamics, 61(9): 1261-1285, 2011.

[27] L. Prandtl, *On the motion of fluids with very little viscosity*. Proc. of the Third Intern. Math. Congr. Heidelberg,1904.

[28] J. Rivlin & R. Wallach, *An analytical solution for the lateral transport of dissolved chemicals in overland flow*, Water Resources Research, **31** (1995), n^o 4, 1031-1040

[29] H. Schlichting. **Boundary-Layer Theory**. McGraw-Hill Book Company, 1968.

[30] F.T. Smith, *Flow through constricted or dilated pipes and channels*. Q.J. Mech. Appl. Math., **29** (1976), 343-364 & 365-376

[31] K. Stewartson. *On the impulsive motion of a flat plate in a viscous fluid*. Q.J. Mech. Appl. Math., **4** (1951), 143-152

[32] L. Tatard, O. Planchon, J. Wainwright, G. Nord, D. Favis-Mortlock, N. Silvera, O. Ribolzi, M. Esteves & Chi-hua Huang. *Measurement and modelling of high-resolution flow-velocity data under simulated rainfall on a low-slope sandy soil*. Journal of Hydrology, 348(1-2): 1-12, 2008.

[33] A.Valiani, V. Caleffii & A. Zanni. *Case study: Malpasset dam-break simulation using a two-dimensional finite volume method*. Journal of Hydraulic Engineering, 128(5): 460-472, 2002.

[34] G. B. Whitham, **Linear and Nonlinear Waves**, Pure and Applied Mathematics, Wiley-Interscience, John Wiley & Sons, New York-London-Sydney, 1974